# CLEAN RESOURCES FINAL PUBLIC REPORT TEMPLATE

## 1. PROJECT INFORMATION:

| | |
|---|---|
| **Project Title:** | **Platform to accelerate the design and use of energy storage solutions from materials scale to microgrid scale** |
| **Alberta Innovates Project Number:** | 232404647 |
| **Submission Date:** | March 29 2026 |
| **Total Project Cost:** | $502 350 |
| **Alberta Innovates Funding:** | $250 000 |
| **AI Project Advisor:** | Amanda Mitchell |

## 2. APPLICANT INFORMATION:

| | |
|---|---|
| **Applicant (Organization):** | **University of Calgary** |
| **Address:** | 2500 University Drive NW, Calgary AB |
| **Applicant Representative Name:** | Arne Dankers |
| **Title:** | Assistant Professor, Schulich School of Engineering, Department of Electrical and Software Engineering |
| **Phone Number:** | 403 220 8196 |
| **Email:** | arne.dankers2@ucalgary.ca |

*Alberta Innovates and His Majesty the King in right of Alberta make no warranty, express or implied, nor assume any legal liability or responsibility for the accuracy, completeness, or usefulness of any information contained in this publication, nor for any use thereof that infringes on privately owned rights. The views and opinions of the author expressed herein does not reflect those of Alberta Innovates or His Majesty the King in right of Alberta. The directors, officers, employees, agents and consultants of Alberta Innovates and The Government of Alberta are exempted, excluded and absolved from all liability for damage or injury, howsoever caused, to any person in connection with or arising out of the use by that person for any purpose of this publication or its contents.*

## A. EXECUTIVE SUMMARY

**Provide a high-level description of the project, including the objective, key results, learnings, outcomes and benefits.**

Microgrids are considered a critical link in the energy transition, facilitating the integration of distributed energy resources (DERs) in the grid's medium and low voltage layers and providing sustainable electrification to remote and isolated communities. Operating microgrids is challenging, given their unique characteristics including system size, tight dynamics coupling, and high penetration of renewable energy sources such as wind and solar. Hence, most microgrids rely on energy storage systems to maintain stability, enhance operational reliability, and increase efficiency.

This multi-disciplinary project aimed to develop a platform connecting material science and power engineering to improve degradation performance of energy storage devices using microgrid operating data. The platform aimed to consist of tools to monitor energy storage device dynamics using real power grid data. The estimated models enabled power engineers to develop degradation models of energy storage devices that reflect actual operating conditions.

Originally, the degradation models were to be embedded in energy management systems to build degradation-aware energy management systems. The estimated models (from the monitoring algorithm) aimed to inform materials scientists about the root causes of degradation of the energy storage system, thereby enabling them to select materials to address the root causes of degradation, and influencing future energy storage device design and management to extend operating life. The project included an artificial intelligence (AI) approach to predict battery properties for given materials and structures, and thereby narrowing down the optimal selection of battery chemistries for future battery development and testing efforts.

Based on the results of efforts undertaken during the project, battery operational costs were reduced by managed by optimizing cycling schedule, thereby prolonging the life of the battery, while still meeting power demands.

The predictive battery material tool demonstrated the feasibility of using artificial intelligence (AI) to select ionic conductivity of different materials and structures with good accuracy. These findings provide a foundation for future development of AI-assisted battery material selection tools based on desired performance parameters.

The learnings of this project have influenced the development of the platform, including degradation considerations for energy management systems (EMS) systems. While monitoring of physical properties of batteries while connected to was not possible as desired due to unexpected issues with the intended test microgrid, modeled elements influenced by real-world data collected from microgrid operations, demonstrates that building such AI-based tools is not only possible but can be effective. Each component will continue to be validated and refined using data from physical devices.

## B. INTRODUCTION

**Please provide a narrative introducing the project using the following sub-headings.**

- **Sector introduction:** Include a high-level discussion of the sector or area that the project contributes to and provide any relevant background information or context for the project.
- **Knowledge or Technology Gaps:** Explain the knowledge or technology gap that is being addressed along with the context and scope of the technical problem.

### Sector Introduction

The quest to achieve ambitious emission reduction targets as set by countries like Canada demands an accelerated shift to renewable power generation and distribution (www.eciu.net, 2024).

Microgrids are considered a critical link in the energy transition, facilitating the integration of distributed energy resources (DERs) in the grid's medium and low voltage layers and providing sustainable electrification to remote and isolated communities. Operating microgrids is challenging, given their unique characteristics including system size, tight dynamics coupling, and high penetration of renewable energy sources such as wind and solar. Hence, most microgrids rely on energy storage systems to maintain stability and enhance operational reliability and efficiency.

The integration of energy storage technologies such as flow batteries, metal-ion batteries, and power-to-hydrogen solutions (such as water electrolysers) into microgrid systems is vital for their further development. The widespread adoption of energy storage technologies in microgrids is hindered limited long-term stability under “live” microgrid operation and associated operating costs. The reason for the lack of stability is two-fold: 1) lack of data on real-world power flow when material scientists design energy storage devices and 2) insufficient understanding of degradation patterns and state of health (SoH) of devices when microgrid operators perform scheduling, adversely affecting the devices' performance, durability, and useful life.

Energy storage devices inevitably degrade over time. Currently degradation of energy storage devices is tested in the lab by subjecting it to repeated charging and discharging cycles. External factors which may impact degradation, such as fluctuating supply and demand, presence of (high frequency switching) power electronics, temperature changes, etc. are not always included in the experimental design. Therefore, the degradation under realistic conditions (which may include rare extreme events) remains largely unknown when designing energy storage devices.

### Knowledge and Technology Gaps

This degradation conundrum creates significant gaps in the development and deployment of energy storage devices for microgrid system applications, resulting in suboptimal designs and management strategies for energy storage devices. This suboptimal design provides opportunity for improving performance, durability, and longevity of batteries to cope with the variable and demanding conditions of real-world applications. Laboratory development of materials and device designs are rarely optimized with demands of real-word variables through data science approaches, and microgrid scheduling algorithms may be inadvertently degrading energy storage devices faster than necessary.

This project proposed to develop an integrated platform connecting energy storage material selection to microgrid performance through real-time degradation monitoring and optimization.

The platform addresses two critical operational challenges:

(1) Microgrid operators lack data on how charge/discharge decisions impact long-term battery health.

(2) Material scientists have limited insight into how material properties influence device degradation under real-world operating conditions.

The project integrated three complementary work areas to create a multi-scale monitoring and optimization framework which focused on microgrid energy management, data driven modeling and parameter identification, and AI guided battery material design.

## C. PROJECT DESCRIPTION INTRODUCTION

**Please provide a narrative introducing the project using the following sub-headings.**

- **Sector introduction:** Include a high-level discussion of the sector or area that the project contributes to and provide any relevant background information or context for the project.
- **Knowledge or Technology Gaps:** Explain the knowledge or technology gap that is being addressed along with the context and scope of the technical problem.

**Technology Development Objectives**

This technology development project focused on a multi-disciplinary approach aimed at integrating material science, data driven models, and power systems engineering.

The objective was to develop a platform to monitor battery degradation during operation in microgrids. The platform was intended to inform materials scientists about battery device degradation physics during operation, thereby informing future longer-life battery design. This platform was also aimed at informing power system engineers about battery degradation from a macro, operational viewpoint, enabling the design of degradation-aware energy management systems from a cost optimization standpoint.

The two key assumptions made for this project included:

1. Microgrid operators lack data on the impact of charge and discharge cycles scheduling on the longevity of operating storage devices, which also influence operating costs.
2. Material scientists lack data regarding real-world battery use in microgrids (fluctuating demand, renewable energy variability, grid interactions, diverse load and generator behaviors, and possible faults) to address weaknesses in functional material design impacting the ability to select optimal materials for robust energy storage devices.

Work for this project was broken down into three different Work Areas and Milestones to develop an integrated framework for battery operation and design from an optimized microgrid operations standpoint, as illustrated in Fig. 1.

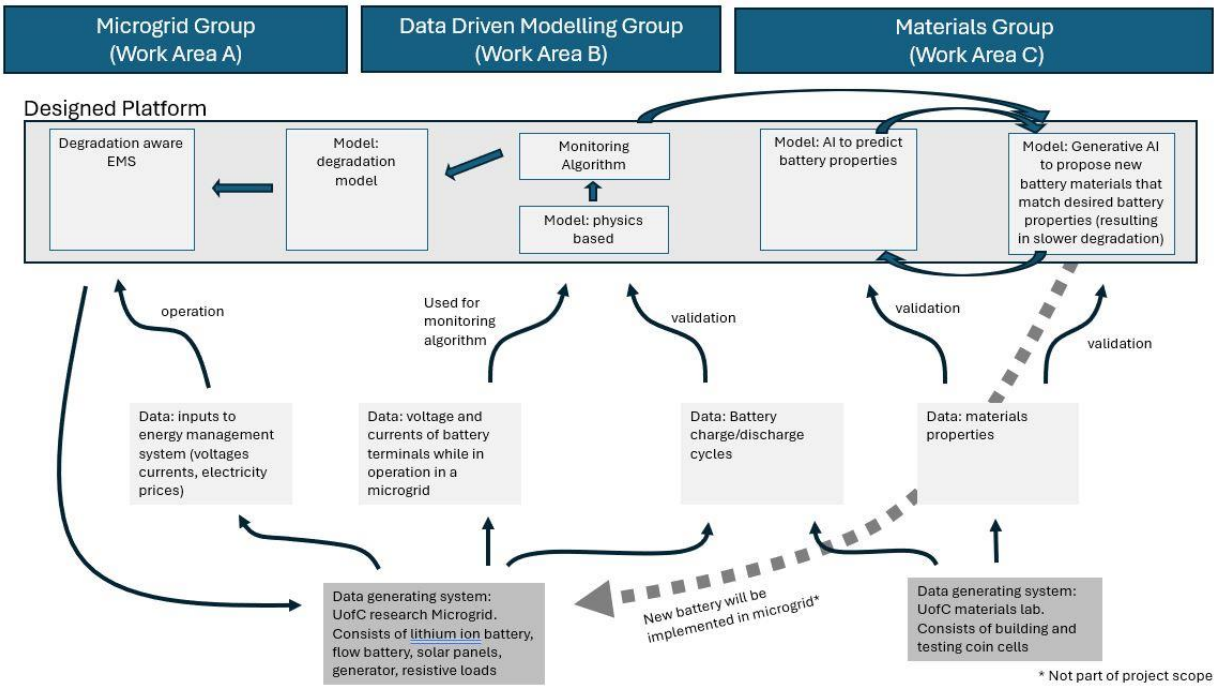



*Figure 1: Graphical Representation of the Proposed Project*

**Work Area A – Degradation-informed scheduling strategies of energy storage devices within a microgrid.**

The objective of this work area was to develop energy-management algorithms for a microgrid that incorporated both the current degradation and predicted future degradation of energy storage devices into their charging and discharging schedules. It was hypothesized that this approach would slow the degradation of the storage devices by operating them in a manner to minimized harm and preserved performance for as long as possible. The final proposed deliverable for this Work Area included a functional, degradation-informed scheduling strategy validated on the University of Calgary's (U of C's) research microgrid.

This scope of work was divided up into the following tasks:

***Microgrid Modelling (Milestone 1)***

This task proposed to focus on building simulation model that matches the University of Calgary campus microgrid, and excluded Faster dynamics were excluded from the scope assuming their impacts would be masked on the direct current (DC) side of the energy storage device (ESS) through the power conditioning system filters.

Subtasks for this work included setting up a simulation environment and adding desired components, and refinements made to the model using empirical data from the research microgrid.

Proposed deliverable: simulator of the microgrid facility at the University of Calgary that generates data and operates in a way the matches the real system in the dynamic range of 0-10Hz (within reasonable tolerances).

***Energy Management Model Selection*** **(Milestone 1)**

This work area aimed top focused on developing degradation-aware energy management systems. The primary technological innovation involved designing algorithms that incorporate battery degradation into the optimization

problem solved by the energy management system at each time step. The resulting optimization framework balanced power flow, system stability, operational cost, and battery degradation to enable more sustainable and efficient microgrid operation.

***Algorithms for Energy Management System (Milestones 2&3)***

The proposed objective of this task included the development of a novel microgrid energy management system that integrates the state of degradation model selected from Task A.1.

Using the microgrid simulator developed in Task 1, an algorithm was proposed to be developed that incorporated the degradation model selected in Task 2. Several algorithms were proposed for testing including a post optimization updating method, a piecewise linear model, and a linear neural network model.

These models were then quantified by incorporating the degradation model into the energy management algorithms and then implemented and tested on the U of C's research microgrid.

***Proposed Deliverables for this Work Area***

Proposed deliverables for this Work Area included:

- A functioning simulator (digital twin) that reasonably matches operations of the microgrid facility at the University of Calgary in the dynamic range of 0-10Hz.
- An algorithm to represent the degradation of energy storage devices including a lithium ion-battery, a vanadium flow battery, and electrolyzer.
- A validated functional degradation- informed algorithm to inform the charge/discharge events of energy storage devices from an operational cost optimization standpoint.

**Work Area B – Data-driven physics-based algorithm development for energy storage devices**

The objective of this work area was to implement data-driven models to estimate the dynamics of energy storage devices during microgrid operation. Newly developed network system identification tools were proposed for use to ensure that the dynamics of the energy storage device could be estimated independently from the broader microgrid dynamics and other system disturbances.

This scope of work was divided up into the following tasks detailed below.

***Model Structure Selection (Milestone 1)***

The proposed objective for this task included the selection of a model structure that could capture the effects of EDM/battery degradation while operating as part of an integrated microgrid.

Simulations of operational data using electrochemical models of ESDs would be used to determine if parameters changes resulted in changes in the specific electromechanical model.

Estimated noise and disturbance elements were to be incorporated and compared to simulation electrochemical model results, thereby estimating "realistic" simulated conditions.

Bench-top experiments were proposed to validate the developed algorithm.

***Monitoring of energy storage device while connected to microgrid (Milestones 2&3)***

The objective of this work area was to develop an algorithm capable of monitoring changes in the dynamics of an energy storage device connected to a microgrid during daily operation. A key innovation of this project was the ability to track the model of the energy storage system while it was actively in use within the microgrid.

To achieve this, an application of network system identification tools was needed to ensure that the dynamics of the energy storage device were estimated independently from those of the microgrid. The model structure selected in Task B.1 would be embedded into a microgrid environment.

Simulation experiments were proposed to estimate the dynamics of the energy storage device separately from those of the microgrid using network system identification tools. A selection of the microgrid variables and control signals would be measured to estimate the physics of the energy storage device.

Subsequently, it was proposed that the network identification tools be implemented and tested using simulation data. Thereby confirming the selected experimental setup and algorithm developed yields consistent estimates of energy storage device dynamics.

The resulting algorithm from these activities was proposed to be implemented and tested on the U of C's experimental microgrid.

***Proposed Deliverables for this Work Area***

Proposed deliverables for this Work Area included:

- An algorithm to map a transfer function representing the dynamics of energy storage devices to a physics-based model.
- An algorithm to estimate the dynamics of an energy storage device using sensor data collected from the microgrid during daily operation.

**Work Area C – Material selection based on the energy storage device physics**

The objective of this work area was to use energy storage systems degradation data from published and experimental microgrid operation to help inform and enable the development of longer-lasting energy storage devices from a materials standpoint. The work completed in this Work Area was proposed to cumulate in an overall degradation-informed material selection framework for battery materials.

***Development of AI guided framework for identification, selection and design of materials for use in energy storage devices (Milestone 1&2)***

The overall objective of this task was to develop an AI-guided framework that used microgrid operational data to support material selection and device design.

A sensitivity analysis to identify which materials design parameters affect energy storage devices using the electrochemical modeling from Work Area B were proposed for use to determine behavioural changes based on material parameters under degradation. Simulations and bench-scaled experiments were proposed to validate these identified material parameters from the sensitivity analysis.

A machine-learning (ML) informed simulation framework for material design was to be developed linking the physics-based electrochemical models with data-driven models estimated from microgrid sensor data.

An artificially intelligent (AI) algorithm to map changes in operational behavior relative to material property degradation was to be developed, which would influence future material selection for energy storage devices/batteries based on desired performance outcomes.

***Design data synthesis for framework (Milestone 2&3)***

This task proposed to focus on designing the data-generation pipeline needed to train and validate the material-design framework.

Critical material design parameters identified in the previous task were to be complied and tracked in the developed AI framework. These material parameters would be validated through simulated and physical experiments on developed energy storage devices/batteries.

***Validation and optimization of developed framework for real-time identification, selection and design of materials in energy storage devices (Milestone 3)***

The objective of this task involved integration all components of this Work Area into a functional, real-time framework capable of linking microgrid sensor data to material-scale design decisions.

Energy storage devices/batteries were to be developed in the previous task could be optimized and these new batteries tested and validated n the experimental microgrid and work completed in Work Area B.

Thereby contributing to the overall envisioned project framework.

***Proposed Deliverables for this Work Area***

Proposed deliverables for this Work Area included:

- Physics based data regarding battery material properties most affected by operating conditions.
- A validated framework for real-time identification, selection and design of energy storage device/battery materials.

**Project and Objectives Updates**

Although many of the project objectives were achieved as planned and proposed, not all planned tasks or objectives could be completed as originally proposed for the project.

The project scope, as proposed, was more ambitious than anticipated in terms of scope, resources and timeline across all Work Areas. As such, some of the key activities and desired steps for the project were adjusted to each Work Area to allow for a focus on a subset of the originally scoped parameters and tasks. As such, The AI generative model could not be fully developed or implemented, and an algorithm to convert the physics-based model into a degradation model for the microgrid group could similarly not be implemented, nor could developed energy management systems (batteries) be validated using the respective models.

The University of Calgary's (U of C's) experimental microgrid malfunctioned early on during the project and could not be fully addressed and rectified within the proposed project timeline and budget. This had a ripple effect on data collection, testing and validation plans across the Work Areas, as testing the developed algorithms and models on a live, integrated microgrid could not proceed as planned. As a result, alternative microgrid operational data was sourced from either from the campus-wide microgrid or an operational utility-scaled microgrid data from a live, industrial-scaled for select model testing and limited validation efforts where possible.

Details about changes to each Work Area and the resulting impacts to the desired framework are detailed below.

**Work Area A: Microgrid Energy Management System (EMS)**

***Algorithms for Energy Management System (Milestones 2&3)***

*Implementation and validation of the Microgrid Model on a Campus-Wide Microgrid*

Originally, the EMS algorithm validation was to be completed using data from the U of C's experimental microgrid, including the use of real energy management devices connected to said microgrid. Because no live data from the U of C's experimental microgrid could be collected, the developed algorithms could not be validated on live energy storage devices as planned.

The campus microgrid includes a Combined Heating and Power (CHP) plant, photovoltaic (PV) generation, and many different loads. The data set consisted of a full year of data including voltage and current measurements of solar panels, loads, price data and weather. This data set allowed for a more practical application of the energy management system by providing a more complex, real data set by which to test the effectiveness of the EMS assumptions and simulations used in the models

*Implementation and validation of the Energy Management System (EMS) Algorithm using Simulated Data*

The issues with the research microgrid resulted in minimal operations data collected for any of the proposed energy management devices (EMDs)/batteries during the project timeline and no ability to test the developed energy management approaches under live operating conditions.

As a result, the simulated physics-based EMDs/batteries developed in Work Area B were used instead. Though the pivot would limit the ability to validate the overall scheduling strategies, it would allow researchers to test different sized simulated EMDs and provide some insights into the scheduling strategies that independent physical testing would not.

*Implement and test the designed algorithm using Simulated EMS and Campus-Wide Power Production Data from the Campus-Wide Microgrid*

The degradation informed scheduling strategy was then implemented and tested using the campus-wide power generation data and the simulated EMS/battery devices developed.

***Updated Deliverables for this Work Area***

Updated deliverables for this Work Area reflective of the scope changes:

- A functioning simulator (digital twin) that reasonably matches operations of the campus microgrid.
- An algorithm to represent the degradation of energy storage devices/batteries developed using physics-based published data.
- A semi-validated functional algorithm to inform the charge/discharge events of energy storage devices from an operational cost optimization standpoint.

**Work Area B – Data-driven physics-based algorithm development for energy storage devices**

With the research microgrid unavailable for use to complete the testing of the developed algorithm on a live, integrated microgrid an alternative approach was proposed. Therefore, objectives and proposed outcomes shifted.

A data set is generated by a 6.5 MW, 40-megawatt-hour (MWh) utility scale microgrid was available to the project team. This microgrid consisted of power generation, a vanadium redox flow battery, and a connected load. Data

collected over 112 days included both voltage and current power electronics measurements at the battery terminals.

Use of the utility-scaled grid data would provide a richer and longer data set than that of the experimental microgrid, it would not allow for different ESDs to be connected to that grid to collect degradation data. Data collection was therefore limited to the vanadium redox flow battery from an operations standpoint.

***Monitoring of energy storage device while connected to microgrid (Milestones 2&3)***

*Implement and test network identification tools using simulation data*

Without long-time operational data from the research microgrid to influence the simulated ESD model development, published data had to be used to either supplement or fully used to develop simulations for lithium-ion and electrolyzer devices.

A lack of published data and insufficient time to analyze and incorporate data from the utility operating grid resulted in an inability to develop a physics-based simulation model for the vanadium flow battery.

*Implement and test network identification tools using simulation data*

From a practical application standpoint, this real-world data set would provide a richer and longer data set than that of the experimental microgrid and would also limit the types of ESD that could be tested and analyzed relative to the rest of the project work.

Operational data was available for the flow battery, but with no simulated flow battery developed as part of Task B.1, and therefore a data-driven algorithm for this device could not be fully developed, tested, nor validated within the project timeline and budget.

Physics based models for electrolyzers were developed and insufficient time and budget limit the number of different energy devices to be modelled, implemented and tested. Therefore, this element was removed from this project's focus.

Because developing a degradation model for a battery requires continuous data collection over a long period of time, which could not be completed due to the microgrid issues, a degradation model for lithium-ion batteries using published data gathered from literature was used for the degradation-aware energy management system. As such, this model could not be fully validated via the research microgrid at the time of project execution.

***Updated Deliverables for this Work Area***

Proposed deliverables for this Work Area included:

- An algorithm to map a transfer function representing the dynamics of a lithium-ion battery to a physics-based model.

Proposed deliverables for this Work Area included:

- An algorithm to map a transfer function representing the dynamics of energy storage devices to a physics-based model.
- A modular model of a power system where new components can be added or removed as part of an overall network structure approach.
- Building a link between a transfer function of a battery and the physics of the battery that would be estimated from data.

- Collection of monitoring the dynamics of energy management systems while connected to a microgrid during normal operation both from published sources and utility-scaled gird operations.

**Work Area C – Material selection based on the energy storage device physics**

The original scope of work as proposed for this Work Area, though less impacted by the loss of the experimental microgrid element, resulted in being overly ambitious in terms of scope, budget, effort and timeline. As such, each task was focused on a more specific and constraint scope.

***Development of AI guided framework for identification, selection and design of materials for use in energy storage devices (Milestone 1&2)***

In the original proposal a generative AI was going to be trained to suggest new battery materials that have properties that slow degradation. This objective turned out to be too ambitious.

*Sensitivity Analysis & Incorporation of Physics-based Model Data Sets*

Without physics-based performance data from the operational research microgrid that was to be provided by Work Area B for this task, the project team used published data and an ML approach to conduct the sensitivity analysis for material parameter identification.

This work was limited to polymer-based (electrolyte) lithium-ion batteries due to the volume of available literature and published data to inform the sensitivity analysis. With a lithium-ion battery being one of the installed ESDs on the original campus, there was early optimism that the research grid could be repaired in time to test and validate the proposed framework.

Though several battery materials properties of import were identified through the sensitivity analysis conductivity was the key property evaluated and semi-validated in this work scope with other properties to be further explored and modelled beyond the scope of this project.

***Validation and optimization of developed framework for real-time identification, selection and design of materials in energy storage devices***

Time and cost of materials to develop coin-scaled batteries resulted in fewer physical batteries developed to test predictive algorithms. Therefore, published data sets in addition to in-house experimental data were used for the predictive model testing and preliminary validation efforts associated with predictive model development.

The work on predictive AI is promising from the validation experiments that have been completed, and a deferral of the generative AI component of the project is required to allow for additional work to populate the AI predictive materials framework as envisioned.

***Updated Deliverables for this Work Area***

Proposed deliverables for this Work Area included:

- A predictive AI model for conductive materials in polymer-based lithium ion-batteries.
- A limited experimentally tested data set for the polymer electrolyte-based lithium-ion batteries validated against a large processed published data set for lithium-ion batteries.

Figure 2 with a graphical representation of the project as completed is shown below reflecting changes made to the project. Components remaining incomplete are shown in brown.

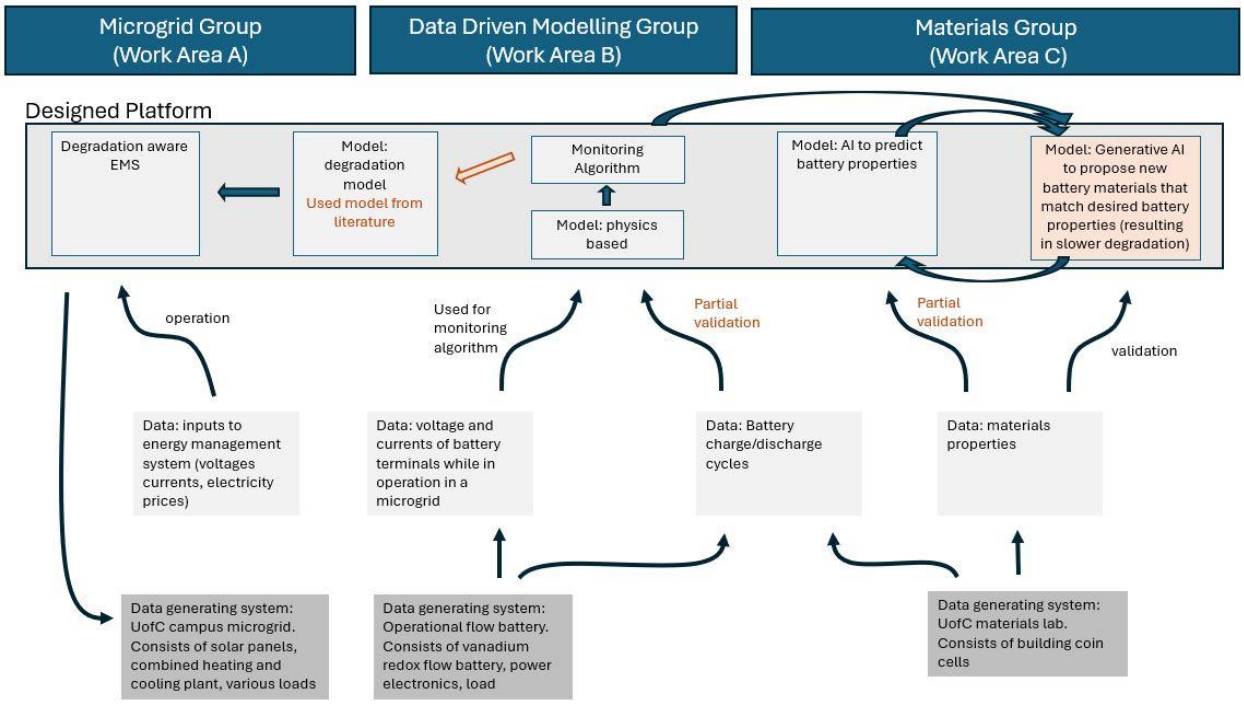



*Figure 2: Graphical Representation of the Project Completed*

**Project Performance Metrics**

The following performance metrics were proposed for the project to align with Alberta Innovates' Clean Resource 2030 Strategic Plan at the time of project proposal:

**TRL advancement:** When the project started, the technology readiness level (TRL) of the technology in all three work areas were at a proof-of-concept level of development aligning with Alberta Innovates' definition of TRL 3 with a proposed completion target of TRL 5, or laboratory validated results, for all three Work Areas.

**Students Trained:** A total of seven students were proposed to be trained as part of this project, including three in energy management system design, two in data-driven modeling and two in data analysis and modeling.

**Publications**: A total of three publications were proposed for the project.

**Knowledge Mobilization:** Three conferences were targeted as part of the project activities including one per Work Area.

**Existing Sector Jobs Retained:** The project proposed to maintain ten highly qualified professional jobs to support project work.

**Technologies Developed in Association with the Project:** Three targeted technologies were proposed with one per Work Area.

## D. METHODOLOGY

**Please provide a narrative describing the methodology and facilities that were used to execute and complete the project. Use subheadings as appropriate.**

*RESPOND BELOW*

The methods and results of the work undertaken as part of the different Work Areas within the project are broken down and detailed below. The project was conducted over three milestone time periods with activities and results of those work periods presented in the following section.

**Work Area A – Degradation-informed scheduling strategies of energy storage devices within a microgrid.**

For this Work Area three distinct degradation modeling methods to accurately represent and incorporate BESS degradation were implemented and compared. The first method is a post-optimization updating method (POUM), in which the degradation coefficient is updated after each day of operation. The second approach employs a PWL approximation of the cycle aging degradation function. Finally, a linearized neural network (LNN) representation of the same degradation function is proposed to capture degradation behavior more accurately.

This research considered the daily optimization of the University of Calgary campus microgrid operation within a mixed integer linear programming framework (MILP), utilizing realistic operational data including campus load, photovoltaic (PV) generation, electricity pool prices from the Alberta Electric System Operator (AESO), and natural gas prices. Furthermore, the end-of-life criteria for the BESS are 70 % of the original capacity (Grimaldi et. al., 2025). The optimization objective was to minimize the annual campus operating cost while accurately accounting for BESS degradation.

The main contributions in this Work Area are summarized as follows:

- Comparative framework for degradation-aware BESS optimization: Developing a comparison of three degradation modeling approaches that model realistic cycle-aging behavior demonstrating the trade-off between computational complexity and optimization optimality and accuracy.
- Linearized neural network for nonlinear degradation embedding: Introduction of a novel method to embed trained NN with ReLU activations directly into mixed integer linear programming (MILP) frameworks, enabling accurate representation of nonlinear degradation dynamics while maintaining optimization linearity and global optimality.
- Degradation-aware operation of campus microgrid with sensitivity analysis: Integration of the proposed methods with the University of Calgary campus microgrid using realistic Alberta market conditions, demonstrating the impact of degradation modeling on BESS scheduling, operational costs, and profitability across different BESS sizes and C-rates.

**Milestone 1**

The work completed for this Work Area during Milestone 1 consisted of microgrid modeling efforts. Aspects of the microgrid modelling work were modified during Milestone 3, when the algorithm was applied to the campus microgrid, but is discussed in this section.

The proposed MILP optimization framework is presented along with the BESS degradation models. In this framework, a daily MILP optimization is developed to minimize the operational cost of the University of Calgary Campus microgrid while accounting for the degradation of the BESS and its impact on the economics and

operation scheduling of the campus resources. The objective function and degradation models are elaborated in the following sections.

The microgrid, or campus microgrid in this case, is shown in Fig. 3., and consisted of five (5) disconnected microgrids, though for the purposes of this project assumed all microgrids were unified and form a single grid-connected microgrid.

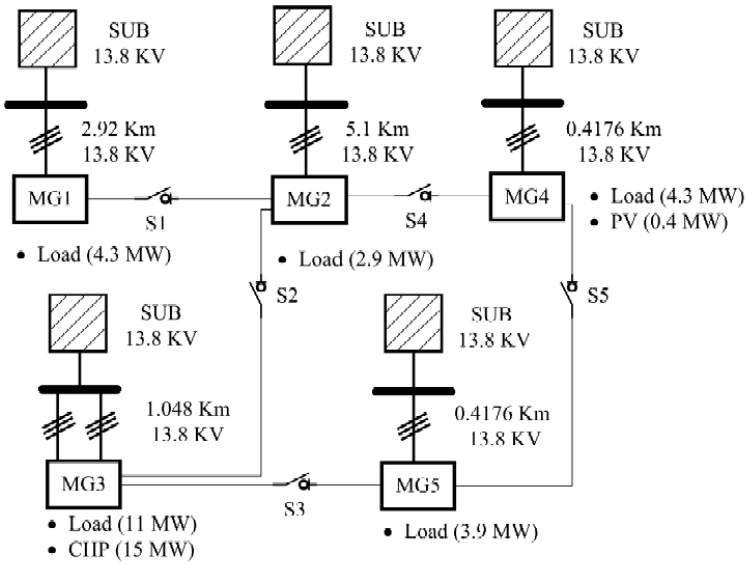



*Figure 3: Schematic diagram of U of C microgrid.*

In this framework a daily MILP optimization was developed to minimize the operational cost of the University of Calgary Campus microgrid while accounting for the degradation of the BESS, and its impact on the economics and operation scheduling of the campus resources. The objective function and degradation models are elaborated in the following sections.

The objective function aimed to minimize the annual campus operational cost, which consists of different components such as the CHP plant generation costs, operation and maintenance (O&M) costs for PV and BESS, the revenue earned by selling power back to the grid, and the cost of purchasing power from the grid along with the degradation cost of the BESS. The mathematical formulation for the objective function, O, is as follows:

$$\min \quad \mathcal{O} = \sum_{d \in \mathcal{D}} \left[ C_d^{\mathrm{CHP}} + C_d^{\mathrm{O\&M}} + C_d^{\mathrm{b}} - C_d^{\mathrm{s}} + C_d^{\mathrm{deg}} \right]$$

where D and d are the set and index for each day.

The operational cost of the campus included the cost of electricity generated by the CHP plant, $C_d^{CHP}$, the operation and maintenance cost for PV and BESS, $C_d^{O\&M}$, the revenue from selling electricity to the grid, $C_d^{S}$, the

cost of purchasing electricity from the grid, $C_d^b$, and $C_d^{deg}$ representing the degradation cost of the BESS. These cost components are represented as follows:

$$C_d^{\mathrm{CHP}} = \sum_{h \in \mathcal{H}} P_h^{\mathrm{CHP}} \times H_h$$

$$C_d^{\mathrm{O\&M}} = \left[ \sum_{h \in \mathcal{H}} P_h^{\mathrm{PV}} c^{\mathrm{PV}} \times + c^{\mathrm{BESS}} \times I^{\mathrm{BESS}} \right]$$

$$C_d^{\mathrm{s}} = \sum_{h \in \mathcal{H}} P_h^{\mathrm{s}} \times \alpha_{\mathrm{pp},h}$$

$$C_d^{\mathrm{b}} = \sum_{h \in \mathcal{H}} C_h'^{\mathrm{b}} + C_d''^{\mathrm{b}}$$

$$C_d^{\mathrm{deg}} = \xi_{\mathrm{deg}} \times \sum_{h} \left( P_h^{\mathrm{ch}} + P_h^{\mathrm{dis}} \right) \times \Delta h$$

where H denotes the set of hours in each day, and $P_h^{CHP}$ is the power generated by the CHP plant in MW and $H_h$ is the heat rate in $/MWh for hour h; $c^{PV}$ is the unit O&M cost of PV in $/MWh and $P_h^{PV}$ is the PV output in MW. In contrast to PV, the BESS O&M cost is fixed throughout the year and is represented by $c^{BESS}$ in $/MW-year; $P_H^s$ h is the power exported to the grid in MW and $\alpha_{pp,h}$ represents the electricity pool price in $/MWh; $C_h'^b$ and $C_d''^{,b}$ represent the hourly and daily electricity purchase costs in $, respectively, which are detailed in the subsequent subsection; $\zeta_{deg}$ is the degradation coefficient in $/MWh, $P_h^{ch}$ and $P_h^{dis}$ are the BESS charging and discharging power in MW, and Δh is the time-step duration in hours.

The electricity market in Alberta operates under a hierarchical structure. The hourly electricity pool price is determined in the spot market by AESO. Subsequently, DFOs apply additional T&D fees and local access fees (LAF). As a result, some components of the electricity bill are calculated hourly, while others, such as demand charges, are calculated daily. The overall hourly component is formulated as follows:

$$C_d'^{\mathrm{b}} = \sum_{h \in \mathcal{H}} \Big( P_h^{\mathrm{b}} \times \alpha_{\mathrm{pp},h} + P_h^{\mathrm{b}} \times \alpha_{\mathrm{on}} \times e_h^{\mathrm{on}} + P_h^{\mathrm{b}} \times \alpha_{\mathrm{off}} \times e_h^{\mathrm{off}} + P_h^{\mathrm{b}} \times \alpha_{\mathrm{laf}} \Big)$$

where $\alpha_{on}$, $\alpha_{off}$, and $\alpha_{laf}$ represent the electricity rates for onpeak and off-peak times, and LAF in $/MWh respectively. Time-of-use (TOU) pricing defines the on-peak period as 8:00 a.m. to 9:00 p.m. on weekdays, excluding weekends and statutory holidays. Other times are considered off-peak. Additionally, $e_h^{on}$ and $e_h^{off}$ are binary parameters that indicate the TOU status of the hour. The electricity bill daily component is as follows:

$$C_d''^{\mathrm{b}} = \alpha_{\mathrm{sc}} + V_d \times \alpha_{\mathrm{nrdc}} + b_d \times \alpha_{\mathrm{fc}} + b_d \times \alpha_{\mathrm{dc}}$$

where $\alpha_{sc}$ denotes the fixed service charge in $, and$\alpha_{nrdc}$, $\alpha_{fc}$, and $\alpha_{dc}$ represent the rates for the Non-Ratchet Demand Charge, Facility Charge, and Demand Charge, respectively, all in $/MVA. Furthermore, $b_d$ and $V_d$ denote the billing demand and the daily peak purchased power in MW. The billing demand is defined as the greater of the daily peak purchased power and 90% of the peak over the previous 365 days, known as the ratchet demand, as follows:

$$b_d = \max\left\{V_d,\ 0.9 \times \max_{d' \in [d-365,\ d-1]} V_{d'}\right\}$$

The billing demand requires identifying the daily peak power, as shown in the following equations. Note that these equations are the linearized form of a maximum function.

$$V_d \geq P_h^{\mathrm{b}}$$

$$V_d \leq P_h^{\mathrm{b}} + (1 - PD_h) \times M$$

$$\sum_{h \in \mathcal{H}} PD_h = 1$$

where $PD_h$ is a binary variable for peak detection and M is a sufficiently large number. Similarly, $b_d$ is linearized as follows:

$$b_d \geq V_d$$

$$b_d \geq P_d^{\mathrm{r}}$$

$$b_d \leq V_d + (1 - BD_d) \times M$$

$$b_d \leq P_d^{\mathrm{r}} + BD_d \times M$$

where $BD_d$ is a binary variable selecting daily peak vs. the ratchet demand, and $P_d^r$ is the historical ratchet demand.

To ensure appropriate interactions with the grid, constraints were added that disallow buying and selling power from/to the grid simultaneously, and imposed an upper limit on the power purchased or sold:

$$u_h^{\mathrm{s}} + u_h^{\mathrm{b}} \leq 1$$

$$P_h^{\mathrm{b}} \leq u_h^{\mathrm{b}} \times P^{\mathrm{b,max}}$$

$$P_h^{\mathrm{s}} \leq u_h^{\mathrm{s}} \times P^{\mathrm{s,max}}$$

where $u_h^s$ and $u_h^b$ are binary variables for selling and buying electricity, respectively. Furthermore, $P^{b,max}$ and $P^{s,max}$ represent the maximum power limits for buying and selling electricity from/to the grid in MW.

The CHP plant output is limited by the upper and lower bounds:

$$P_h^{\text{CHP}} \leq P^{\text{CHP,max}} \times u_h^{\text{on}}$$

$$P_h^{\text{CHP}} \geq P^{\text{CHP,min}} \times u_h^{\text{on}}$$

where $P^{CHP,max}$ and $P^{CHP,min}$ represent the maximum and minimum CHP plant output power in MW. Ramp-up and ramp-down limitations are enforced by

$$P_h^{\text{CHP}} - P_{h-1}^{\text{CHP}} \leq P^{\text{ru}}$$

$$P_{h-1}^{\text{CHP}} - P_h^{\text{CHP}} \leq P^{\text{rd}}$$

Where $P^{ru}$ and $P^{rd}$ represent the rampdown and ramp-up limits in MW/h. The number of times the CHP plant can be turned off during its operation is restricted by:

$$\sum_{i=1}^{24} 1 - u_i^{\text{on}} \leq T^{\text{off}}$$

The constraints ensured that the minimum uptime and downtime requirements of the plant were satisfied:

$$\sum_{i=h}^{\min(h+T^{\text{u}}-1,\,|\mathcal{H}|)} u_i^{\text{on}} \geq (\min(T^{\text{u}},\,|\mathcal{H}|-h+1)) \times \left(u_h^{\text{on}} - u_{h-1}^{\text{on}}\right)$$

$$\sum_{i=h}^{\min(h+T^{\text{d}}-1,\,|\mathcal{H}|)} 1 - u_i^{\text{on}} \geq \left(\min(T^{\text{d}},\,|\mathcal{H}|-h+1)\right) \times \left(u_{h-1}^{\text{on}} - u_h^{\text{on}}\right)$$

where $|H|$ denotes the number of hours in a day, while $T^{off}$ , $T^{u}$ and $T^{d}$ are the allowable off-times, minimum uptime, and downtime requirements in hours and $u_h^{on}$ is a binary variable which indicates whether the CHP plant is on or off.

**Milestone 2**

The two main tasks completed during this milestone included the selection of a model to capture the degradation of a battery, and the development of algorithms incorporating degradation into the MILP optimization problem. The MILP optimization aspect is explored more fully in the discussion for Milestone 3.

The battery degradation model is a cycle-aging degradation model for lithium-ion batteries which represents the battery capacity as a function of cumulative cycles (Grimaldi et. al., 2025):

$$\begin{aligned} C(cyc) = {} & 100 - 5.613 \times 10-32\, cyc_9 + 3.121 \times 10-27\, cyc_8 - 6.353 \times 10-23\, cyc_7 \\ & + 6.630 \times 10-19\, cyc_6 - 3.987 \times 10-15\, cyc_5 + 1.435 \times 10-11\, cyc_4 \\ & - 3.070 \times 10-8\, cyc_3 + 3.746 \times 10-5\, cyc_2 - 0.0277\, cyc \end{aligned} \quad (1)$$

where $cyc$ is the number of battery cycles as is calculated based on battery throughput:

$$cyc = \frac{\sum_{h\in H}\left(P_h^{ch} + P_h^{dis}\right) \times \Delta h}{2 \times E^{tot}} \tag{2}$$

where $P_h^{ch}$ and $P_h^{dis}$ denote charging and discharging power in MW, $E^{tot}$ is daily capacity in MWh, Δh is the time-step duration in hours, and H is the set of hours in each day.

A simple model was selected in order test the system effectively (run simulations in a reasonable amount of time) and to interpret the results without additional complicating factors. The advantage of this constructed framework is that it allows future, more complex battery degradation models to be added or exchanged with minimal changes. Thus, allowing for consideration such as temperature or load dynamics to be added or considered.

The degradation coefficient quantified the cost of capacity loss per unit throughput:

$$\xi_{\text{deg}} = \frac{\Delta C \times E_{\text{tot}}}{100 \times \Theta_{\text{total}}} \times C^{\text{penalty}}$$

$$C^{\text{penalty}} = \frac{\text{CAPEX}}{L_{\text{expected}}} \tag{3}$$

where $\Delta C = C_{d-1}^{start} - C_{d-1}^{end}$ denotes the daily BESS capacity loss in percentage, $\Theta_{total} = \sum_{h\in H}\left(P_h^{ch} + P_h^{dis}\right)\Delta h$ represents the total energy throughput in MWh, and $C^{penalty}$ is the penalty cost in CAD/MWh; CAPEX is the capital cost of the BESS in CAD/kW, and $L_{expected}$ is the expected lifetime of the BESS, assumed to be 15 years in this case.

To calculate the BESS cost of degradation the total daily throughput of the BESS is multiplied by the BESS degradation coefficient:

$$C_d^{\text{deg}} = \xi_{\text{deg}} \times \Theta_{\text{total}}$$

In this study, the EOL and BESS lifetime were assumed to be 70 % and 15 years respectively. A 2% annual cap on the capacity fade is enforced:

$$\text{C}_\text{d} \geq 98$$

To track the energy stored in the BESS, constraints were added to update the BESS energy state over time:

$$E_h^{\text{stored}} = E_{h-1}^{\text{stored}} + \left(\eta \times P_h^{\text{ch}} - \frac{P_h^{\text{dis}}}{\eta}\right)$$

prevent simultaneous charging and discharging by employing the binary variables $I_h^{ch}$ and $I_h^{dis}$, which indicated whether the BESS operated in charging or discharging mode, respectively:

$$I_h^{\text{ch}} + I_h^{\text{dis}} \leq 1$$

imposing upper bounds on the charging and discharging powers of the BESS:

$$P_h^{\mathrm{ch}} \leq I_h^{\mathrm{ch}} \times P^{\mathrm{ch,max}}$$

$$P_h^{\mathrm{dis}} \leq I_h^{\mathrm{dis}} \times P^{\mathrm{dis,max}}$$

**Milestone 3**

The work completed during Milestone 3 included the continuation and completion of algorithms developed to incorporate degradation into the energy management system. Three degradation-aware energy management systems were implemented.

In the first one, the battery capacity was updated at the end of each day based on that day's usage. This method is referred to as the post-optimization updating method (POUM) and resulted in suboptimal performance due to continuous degradation not considered. The second approach approximated the degradation function as a piecewise linear function (PWL) and the third approach approximated the degradation function as a linearized neural network (LNN).

The key consideration when designing the energy management systems included that the approach must be structured in such a way to fit in a MILP framework. Essentially, the challenge is to represent the degradation function in such a way that it is possible to integrate it into a MILP, and thus it must be expressed in such a way that it is linear in the variables.

***Post-Optimization Updating Method (POUM)***

In the POUM, the BESS degradation coefficient was calculated after each optimization day and incorporated into the subsequent day's optimization. In this post-optimization approach, the capacity loss and total daily throughput were calculated using equations (1) and (2), respectively, and the degradation coefficient is subsequently obtained using (3). This approach inherently uses the previous day's degradation coefficient for the current day's BESS scheduling, which may lead to suboptimal results as it does not account for each day's unique operational requirements and conditions.

***Piecewise Linear Method (PWL)***

In the PWL method, the approach to integrate degradation into the EMS (i.e. the MILP) was to model degradation as a piecewise linear function. Specifically, to perform simultaneous optimization of EMS operations and degradation costs, a piecewise linear approximation of the polynomial degradation function in (1) as a function of battery cycles ($cyc$) was embedded directly into the MILP formulation. The model uses three linear segments as shown in Fig. 4. Note that to fit (1) accurately only 3 linear segments were used, although for more complex functions, more than three segments may be used.

From a framework point of view, this is not a fundamental change, it is simply a practical implementation detail. From Fig. 4. it is observable that piecewise linear function closely approximates the polynomial (1). The key point is that a piecewise linear function is represented using 3 linear in the parameter functions, and 6 linear inequalities, which means that it is possible to implement it directly into a MILP. Specifically, the PWL function is incorporated into the MILP as follows.

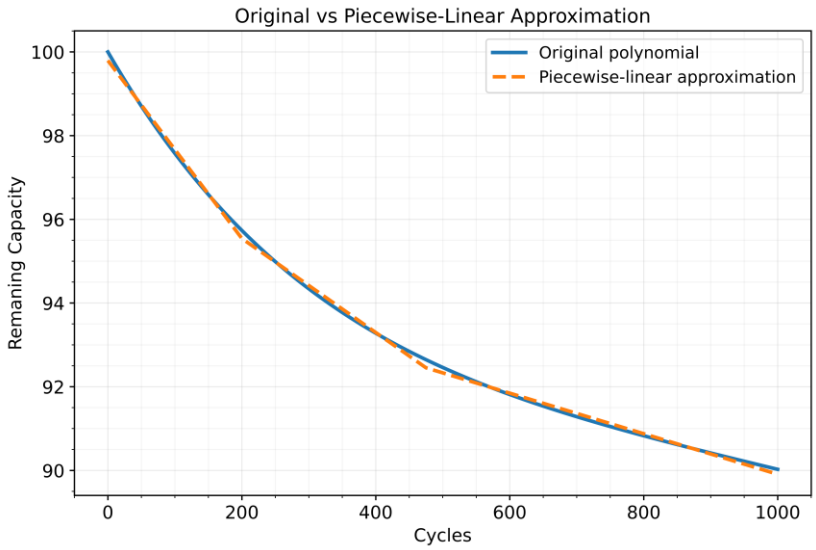



*Figure4 -piecewise linear approximation of (1).*

The piecewise linear function is expressed as:

$$PLW(cyc) = \begin{cases} b_1 + m_1\,cyc, & c_0 \le cyc < cyc_1 \\ C_{200} + m_2\,(cyc - cyc_1), & cyc1 \le cyc < cyc2 \\ C_{475} + m_3\,(cyc - cyc_2), & cyc \ge cyc2 \end{cases}$$

where, $cyc_1$, $cyc_2$ are the ranges for which each linear segment is used (in this case $cyc_1$=200 and $cyc_2 = 475$), $m_1$, $m_2$, $m_3$ are the slopes of the linear segments, and $b_1$, $C_{200} - m_2 cyc_1$, and $C_{475} - m_3 cyc_2$ are the y-intercepts. The piecewise linear function is implemented using binary variables to select the active segment:

$$\sum_{i=1}^{3} s_i = 1, s_i \in \{0,1\}$$

where $s_i$ indicates whether segment $i$ is active. The cycle bounds for each segment are enforced using constraints:

$$cyc \ge 0s_1 + 200s_2 + 475s_3$$

$$cyc \le 200\,s_1 + 475s_2 + 1000s_3.$$

The values for each variable are listed in Table 1.

PIECEWISE LINEAR DEGRADATION MODEL PARAMETERS

| Parameter | Symbol | Value |
|---|---|---|
| Initial Capacity | $b_1$ | 100.00 |
| Breakpoint 1 | $cyc_1$ | 200 |
| Breakpoint 2 | $cyc_2$ | 475 |
| Slope Segment 1 | $m_1$ | $-0.02126$ |
| Slope Segment 2 | $m_2$ | $-0.01124$ |
| Slope Segment 3 | $m_3$ | $-0.00485$ |
| Capacity at 200 cycles | $C_{200}$ | 95.75 |
| Capacity at 475 cycles | $C_{475}$ | 92.66 |

*Table 1 Piecewise linear degradation model parameters*

The third approach implemented was to integrate the degradation model (1) into a MILP using a Linearized Neural Network. In this approach, equation (1) was approximated by a neural network with a single hidden layer

consisting of four neurons and rectified linear unit (ReLU) activation functions. The network takes the cumulative cycle count, denoted by $cyc$, as its input and outputs the predicted battery capacity $C_d$ expressed in percent.

The input is first normalized according to

$$\tilde{x} = \frac{cyc}{X_{scale}}$$

where $X_{scale}$ is the input scaling factor. The pre-activation value of hidden neuron i is then computed as

$$h_i = w_{i,1}^{(1)}\tilde{x} + b_i^{(1)}, i = 1, \dots, 4.$$

Each hidden neuron applies a ReLU activation,

$$\hat{h}_i = \max(0, h_i),$$

and the normalized network output is obtained as

$$\tilde{y} = \sum_{i=1}^{4} w_{1,i}^{(2)}\ \hat{h}_i + b_1^{(2)}.$$

In the end, the actual predicted battery remaining capacity is calculated through output denormalization as

$$C_{pred} = \tilde{y}\sigma_y + \mu_y.$$

To embed the neural network within a MILP framework, the ReLU activation is reformulated using binary variables δi ∈ {0, 1} and the big M technique. For each hidden neuron i, the ReLU behavior is enforced by the following linear constraints:

$$\hat{h}_i \geq 0,$$

$$\hat{h}_i \geq h_i,$$

$$\hat{h}_i \geq h_i + M_i(1 - \delta_i),$$

$$\hat{h}_i \geq M_i\delta_i.$$

The values used for the parameters in the LNN model are shown in Tables 2 and 3. These were obtained by fitting the output of the neural network to the output of the function (1).

NEURAL NETWORK WEIGHTS AND BIASES

| Layer | Weights $W$ | Biases $b$ |
|---|---|---|
| Hidden Layer | $w_{1,1}^{(1)} = 1.2472$ | $b_1^{(1)} = -0.5906$ |
| | $w_{2,1}^{(1)} = 1.7443$ | $b_2^{(1)} = 0.0902$ |
| | $w_{3,1}^{(1)} = -1.7835$ | $b_3^{(1)} = 0.3253$ |
| | $w_{4,1}^{(1)} = -0.2332$ | $b_4^{(1)} = 0.2349$ |
| Output Layer | $w_{1,1}^{(2)} = 1.3611$ | $b_1^{(2)} = 0.4141$ |
| | $w_{1,2}^{(2)} = -1.6619$ | |
| | $w_{1,3}^{(2)} = 1.7005$ | |
| | $w_{1,4}^{(2)} = 0.2347$ | |

*Table 2: Neural Network Weights and Biases*

$\mathcal{M}$ VALUES FOR RELU LINEARIZATION

| Neuron | Big-M Value ($M_i$) |
|---|---|
| 1 | 1.3131 |
| 2 | 3.6691 |
| 3 | 2.9164 |
| 4 | 0.4698 |

*Table 3: Values for ReLU Linearization*

This research work was based on realistic data from the University of Calgary campus microgrid and the Alberta electricity market. The annual load and PV generation profiles for the University of Calgary campus are depicted in Figures 5 and 6. Figure 7 illustrates the electricity pool price (AESO, 2023). The BESS costs data are sourced from the National Renewable Energy Laboratory (NREL., 2024).

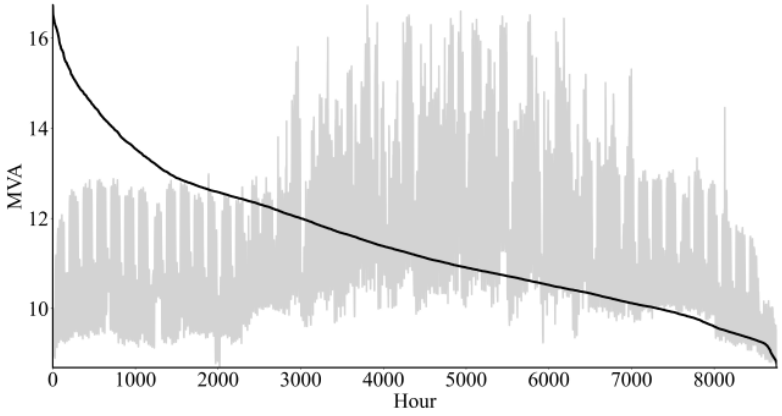



*Figure 5: Campus load profile and its duration curve.*

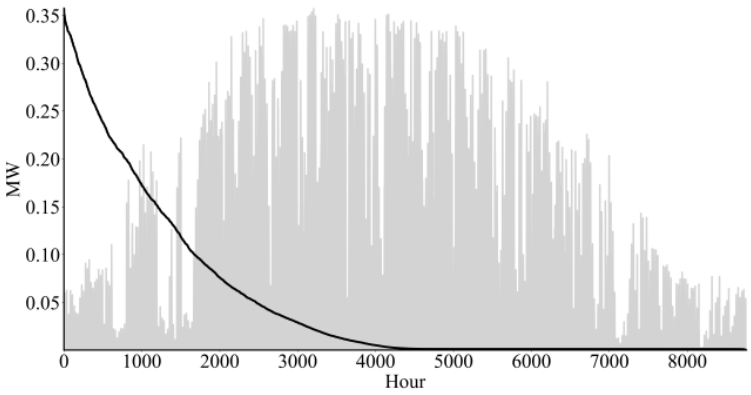



*Figure 6: PV generation profile and its duration curve.*

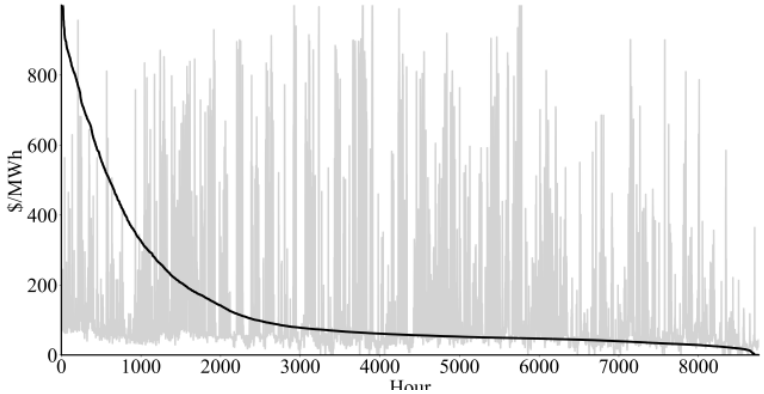



*Figure 7: Alberta electricity pool price and its duration curve*

The numerical results for baseline configurations are presented in Table 4.

The analysis shows that for identical battery sizes, the operating costs with depreciation remain nearly constant across different battery degradation modeling approaches, with negligible variations attributed to solver noise. However, differences exist in capacity loss and battery depreciation costs among the various methods (which would lead to higher overall costs from a replacement standpoint). These discrepancies are due to the inaccuracies inherent in NN and PWL predictions, which cause the battery to operate beyond the 2% annual capacity degradation cap. Regarding computational efficiency, the POUM approach demonstrates shorter solve times due to its simplified formulation and fewer constraints.

A comprehensive sensitivity analysis was conducted across varying battery sizes and C-rates, with results presented in Table 5, Table 6, and Table 7. This analysis reveals that increasing battery size extends the EOL timeline, as larger capacities increase the penalty cost, imposing higher degradation costs that discourage BESS utilization. However, the LNN method consistently achieves significantly longer EOL periods than PWL and POUM across all scenarios.

For instance, at a C-rate of 0.25 with a 10 MWh BESS, the EOL day for PWL and POUM reach only 109 and 101 days, respectively, whereas the LNN approach achieves 245 days which is more than double the other methods. This advantage is emphasized at higher C-rates. At C-rates of 0.5 and 1.0, the LNN method extends EOL beyond 365 days, substantially outperforming PWL and POUM, which achieve EOL of 104 and 101 days (C-rate 0.5) and 137 and 130 days (C-rate 1.0), respectively. These results demonstrate the superiority of the LNN approach in optimizing BESS degradation.

Regarding economic performance, the LNN method achieves lower operating costs with depreciation compared to alternative approaches. In Table 5, operating costs remain nearly identical across all degradation modeling methods for battery sizes up to 6 MWh. However, for 8- and 10-MWh systems, the LNN approach yields noticeably lower costs, reducing overall campus operating expenses by 2.6%. Similar trends are seen in Table 6 and Table 7. At a C-rate of 0.5, operating costs with depreciation are comparable across methods for BESS sizes up to 4 MWh. Beyond this, the LNN approach achieves cost reductions of up to 2.7% annually. At a C-rate of 1.0, LNN demonstrates cost advantages for battery sizes exceeding 2 MWh. Notably, for a 10 MWh system, the LNN method achieves cost reductions of $500K and $400K compared to PWL and POUM, respectively.

In summary, these comprehensive results establish the LNN method as superior to both POUM and PWL approaches for integration into linear optimization frameworks. The LNN approach significantly extends BESS lifetime and maintains comparable computational efficiency with negligible differences in solver runtimes. These combined advantages make LNN the preferred method for BESS degradation modeling in energy management systems.

TABLE VII
COMPARISON OF BASELINE CONFIGURATIONS FOR BESS DEGRADATION

| Method | Battery Config. | Capacity Loss (%) | EOL Day | Battery Depreciation Cost ($) | Operating Cost with Depreciation ($) | Solve Time |
|---|---|---|---|---|---|---|
| LNN | 1MW / 4MWh | 2.14 | 88 | 193,375.77 | 4,384,418.36 | 2m 49.1s |
| PWL | 1MW / 4MWh | 2.30 | 87 | 207,833.77 | 4,392,653.53 | 2m 25.1s |
| POUM | 1MW / 4MWh | 2.02 | 79 | 182,532.27 | 4,383,297.80 | 2m 1.7s |

*Table 3: Comparison of baseline configuration for BESS degradation*

TABLE VIII
OPERATING COST FOR DIFFERENT BESS SIZES AND DEGRADATION APPROACHES AT 0.25 C-RATE

| Method | Battery Size (MWh) | Capacity Loss (%) | EOL Day | Operating Cost with Depreciation |
|---|---|---|---|---|
| LNN | 2 | 2.14 | 75.00 | 4,299,425.009 |
| | 4 | 2.14 | 83.00 | 4,369,960.204 |
| | 6 | 2.14 | 103.00 | 4,422,373.013 |
| | 8 | 2.14 | 162.00 | 4,426,836.064 |
| | 10 | 2.14 | 245.00 | 4,449,393.403 |
| PWL | 2 | 2.30 | 79.00 | 4,302,450.184 |
| | 4 | 2.30 | 86.00 | 4,378,211.667 |
| | 6 | 2.30 | 100.00 | 4,443,050.611 |
| | 8 | 2.30 | 103.00 | 4,507,185.175 |
| | 10 | 2.30 | 109.00 | 4,569,207.180 |
| POUM | 2 | 2.01 | 71.00 | 4,296,233.473 |
| | 4 | 2.02 | 79.00 | 4,368,868.140 |
| | 6 | 2.01 | 85.00 | 4,431,421.999 |
| | 8 | 2.01 | 90.00 | 4,494,684.567 |
| | 10 | 2.01 | 101.00 | 4,537,878.859 |

*Table 4: Operating cost for different BESS sizes and degradation approaches at 0.25 C-rate.*

TABLE IX
OPERATING COST FOR DIFFERENT BESS SIZES AND DEGRADATION APPROACHES AT 0.5 C-RATE

| Method | Battery Size (MWh) | Capacity Loss (%) | EOL Day | Operating Cost with Depreciation |
|---|---|---|---|---|
| LNN | 2 | 2.14 | 62.00 | 4,368,376.493 |
| | 4 | 2.14 | 74.00 | 4,498,162.386 |
| | 6 | 2.14 | 133.00 | 4,576,787.546 |
| | 8 | 2.14 | 236.00 | 4,653,905.336 |
| | 10 | 1.83 | $> 365$ | 4,731,827.012 |
| PWL | 2 | 2.30 | 64.00 | 4,374,598.065 |
| | 4 | 2.30 | 74.00 | 4,517,437.488 |
| | 6 | 2.30 | 83.00 | 4,641,645.846 |
| | 8 | 2.30 | 87.00 | 4,773,170.356 |
| | 10 | 2.30 | 104.00 | 4,867,696.164 |
| POUM | 2 | 2.01 | 60.00 | 4,361,919.708 |
| | 4 | 2.02 | 68.00 | 4,492,042.521 |
| | 6 | 2.03 | 76.00 | 4,616,594.196 |
| | 8 | 2.01 | 85.00 | 4,716,825.236 |
| | 10 | 2.01 | 101.00 | 4,801,981.330 |

*Table 5: Operating cost for different BESS sizes and degradation approaches at 0.25 C-rate*

TABLE X
OPERATING COST FOR DIFFERENT BESS SIZES AND DEGRADATION APPROACHES AT 1 C-RATE

| Method | Battery Size (MWh) | Capacity Loss (%) | EOL Day | Operating Cost with Depreciation |
|---|---|---|---|---|
| LNN | 2 | 2.14 | 60.00 | 4,498,654.572 |
| | 4 | 2.14 | 109.00 | 4,726,345.124 |
| | 6 | 2.14 | 237.00 | 4,935,561.066 |
| | 8 | 1.55 | $> 365$ | 5,009,084.923 |
| | 10 | 0.95 | $> 365$ | 4,981,699.603 |
| PWL | 2 | 2.30 | 62.00 | 4,513,737.390 |
| | 4 | 2.30 | 75.00 | 4,785,747.344 |
| | 6 | 2.30 | 92.00 | 5,037,198.816 |
| | 8 | 2.30 | 111.00 | 5,265,961.842 |
| | 10 | 2.30 | 137.00 | 5,489,501.603 |
| POUM | 2 | 2.03 | 59.00 | 4,488,434.566 |
| | 4 | 2.01 | 69.00 | 4,734,287.768 |
| | 6 | 2.02 | 86.00 | 4,961,815.572 |
| | 8 | 2.01 | 104.00 | 5,171,412.744 |
| | 10 | 2.02 | 130.00 | 5,384,463.055 |

*Table 6: Operating cost for different BESS sizes and degradation approaches at 0.25 C-rate*

Classification: Protected A

**Work Area B – Data-driven physics-based algorithm development for energy storage devices**

The objective in this work area was to estimate physical properties of the energy storage devices during operation in a microgrid from data. The objective is split into two sub-objectives. First, develop a mapping from a transfer function of a battery to a physics-based model that contains physical parameters. Then develop an algorithm to consistently (i.e. without bias) estimate the dynamics of a battery while it is connected to a microgrid.

**Milestone 1**

During this milestone, a physics-based model of a lithium-ion battery was selected to enable the derivation of a non-linear state-space model from which properties of the battery can be inferred from the state-space model.

There are many physics-based models presented in the literature. In this work, the model needed to be detailed enough to accurately capture the dynamics of the battery, but simple enough to represent as a transfer function. The Single Particle Model with Electrolyte dynamics (SPMe) appears to strike this balance. In the following text, the SPMe is presented, ending with a state-space representation of the equations.

The SPMe is a reduced electrochemical model of a lithium-ion battery was derived from the Doyle-Fuller-Newman (DFN) model (Marti-Florences et. al, 2023), (Brosa Planella et al, 2022), (Moura et al, 2017). A representation of a battery using the SMPe is shown in Figure 8. In the SPMe the electrodes are represented using single spherical particles surrounded by electrolyte and between electrodes there is a separator. Lithium diffuses in the solid phase electrodes and in the electrolyte.

The Butler-Volmer equation represent the electrical current through the electrodes depending on the voltage difference between the electrode and the electrolyte. A key conceptual feature is that SPMe decouples the microscale (radius of particles) from the macroscale (distance between electrodes), yielding a computationally cheaper model than DFN while capturing electrolyte effects absent in the SPM (Brosa Planella et al, 2022).

Consider the following building blocks used to form the SPMe, following (Moura et al, 2017), with each electrode k ∈ {n, p}, the intercalated lithium concentration $c_s^k(r,t)$ evolving via spherical diffusion:

$$\frac{\partial c_{\mathrm{s}}^k}{\partial t}(r,t) = \frac{1}{r^2}\frac{\partial}{\partial r}\left(D_{\mathrm{s}}^k\, r^2 \frac{\partial c_{\mathrm{s}}^k}{\partial r}(r,t)\right). \tag{4}$$

The boundary conditions (symmetry at center, flux at surface) includes:

$$\left.\frac{\partial c_{\mathrm{s}}^k}{\partial r}\right|_{r=0} = 0,$$
$$\left.\frac{\partial c_{\mathrm{s}}^k}{\partial r}\right|_{r=R_{\mathrm{s}}^k} = -\frac{1}{D_{\mathrm{s}}^k}\, j_{\mathrm{n}}^k(t),$$

With the concentration of lithium at the surface of the electrode as:

$$c_{\mathrm{s,ss}}^k(t) = c_{\mathrm{s}}^k(R_{\mathrm{s}}^k, t).$$

These equations are the standard DFN solid diffusion relations that SPMe retains. The main assumption in the SPMe is that each electrode is approximated as a single particle (Brosa Planella et al, 2022), (Moura et al, 2017).

The electrolyte concentration dynamics across the cell were modelled as follows. Across the through-cell coordinate x (electrode/separator domains), electrolyte concentration $c_e(x,t)$ evolves as (Moura et al, 2017).

$$\varepsilon_{\mathrm{e}} \frac{\partial c_{\mathrm{e}}}{\partial t}(x,t) = \frac{\partial}{\partial x}\left(D_{\mathrm{e,eff}} \frac{\partial c_{\mathrm{e}}}{\partial x}(x,t)\right) + \frac{1-t_+^0}{F} \frac{\partial i_{\mathrm{e}}}{\partial x}(x,t), \tag{5}$$

The interfacial reaction current density uses Butler-Volmer kinetics (Moura et al, 2017):

$$j_{\mathrm{n}}^k = \frac{1}{F} i_0^k \left(\exp\left(\frac{\alpha_a F}{RT}\eta^k\right) - \exp\left(-\frac{\alpha_c F}{RT}\eta^k\right)\right),$$

where exchange current density $i_0$ is defined as

$$i_0^k = k^k \left(c_{\mathrm{s,ss}}^k\right)^{\alpha_c} \left(c_{\mathrm{e}}\right)^{\alpha_a} \left(c_{\mathrm{s,max}}^k - c_{\mathrm{s,ss}}^k\right)^{\alpha_a},$$

and overpotential $\eta$ is defined as

$$\eta^k = \phi_{\mathrm{s}}^k - \phi_{\mathrm{e}} - U^k(c_{\mathrm{s,ss}}^k) - F R_{\mathrm{f}}^k j_{\mathrm{n}}^k.$$

For this project, the transfer function model of the battery was estimated from data. Therefore, the SPMe equation presented above had to be converted into a transfer function model. The following text demonstrates how the SPMe was represented using state space equations, with the conversion from state-space to transfer function being trivial. The state-space form of the SPMe was:

$$\dot{\boldsymbol{x}} = A\boldsymbol{x} + B\, I(t).$$

Where $\dot{x}$ is the state, $I$ is the current selected as the 'input', and $A$ and $B$ were the state space matrices.

To transform the partial differential equation of the SPMe into a state-space representation, the spatial derivative was approximated as a first order difference. The states were then the concentrations of lithium in each discretized spatial region.

In the equations below, the anode and cathode were each split into 4 discrete spatial regions, and the electrolyte was split into 6 discrete spatial regions. The number of spatial regions used to represent each component could be changed with choices between 2-20 spatial regions being common in literature reviewed. For simplicity, the number of regions selected were very small, and it was noted that the data fit well for even small choices. Thus, the state vector was as follows:

$$\boldsymbol{x} = \begin{bmatrix} \boldsymbol{c}_n \\ \boldsymbol{c}_p \\ \boldsymbol{c}_e \end{bmatrix} \in \mathbb{R}^{14}, \qquad \boldsymbol{c}_n \in \mathbb{R}^4,\ \boldsymbol{c}_p \in \mathbb{R}^4,\ \boldsymbol{c}_e \in \mathbb{R}^6,$$

Where $c_n$, $c_p$ and $c_e$ were the concentrations in each spatial region of the negative electrode, positive electrode and electrolyte respectively with the Finite Volume Method is used for spatial discretization.

From (4), the resulting state-space equations for the for the anode and cathode of the SPMe are (Marti-Florences et. al, 2023):

$$\dot{c}_k = A_k\, c_k + B_k\, I(t), \qquad k \in \{n, p\}.$$

where

$$A_k = s_k \begin{bmatrix} -24 & 24 & 0 & 0 \\ 16 & -40 & 24 & 0 \\ 0 & 16 & -40 & 24 \\ 0 & 0 & 16 & -16 \end{bmatrix},$$

where $s_k = D_s^k / \left(R_s^k\right)^2$ and the input enters only at the surface control volume (the boundary spatial elements):

$$B_n = \begin{bmatrix} 0 \\ 0 \\ 0 \\ -\dfrac{6}{R_{\mathrm{s}}^n} \dfrac{1}{F\, a_{\mathrm{s}}^n\, A\, L_n} \end{bmatrix}, \qquad B_p = \begin{bmatrix} 0 \\ 0 \\ 0 \\ +\dfrac{6}{R_{\mathrm{s}}^p} \dfrac{1}{F\, a_{\mathrm{s}}^p\, A\, L_p} \end{bmatrix},$$

Similarly, the electrolyte PDE (5) was discretized across the negative electrode, separator, and positive electrode. The implementation uses 6 discrete spatial regions, two per region. This preserved diffusion coupling between neighboring control volumes; continuity-like coupling at interfaces negative-separator, separator-positive); source terms in electrodes proportional to $(1 - t_+^0)I(t)$, and no source term in the separator (Marti-Florences et. al, 2023), (Moura et al, 2017). The discretized electrolyte dynamics take the form (Marti-Florences et. al, 2023)

$$\dot{c}_e = A_e\, c_e + B_e\, I(t),$$

where $A_e$ is tridiagonal matrix and $B_e$ injected current forcing only in the electrode-side electrolyte control volumes:

$$B_e = \begin{bmatrix} s_1 \\ s_1 \\ 0 \\ 0 \\ s_3 \\ s_3 \end{bmatrix}, \qquad s_1 = -\frac{(1 - t_+^0)}{F\, A\, L_n\, \varepsilon_{\mathrm{e}}}, \quad s_3 = +\frac{(1 - t_+^0)}{F\, A\, L_p\, \varepsilon_{\mathrm{e}}},$$

Putting the state-space models for the anode, cathode and electrolyte together resulted in the final state-update equation for the state space representation:

The output equation is presented below in which the output was the terminal voltage. The terminal voltage in the DFN/SPMe framework was the difference of solid potentials at the current collectors (Moura et al, 2017):

$$V(t) = \phi_{\mathrm{s}}^{+}(0^+, t) - \phi_{\mathrm{s}}^{-}(0^-, t).$$

The general form of the output equation included:

$$V_{\mathrm{cell}} = \underbrace{\left(U^p(\theta_p) - U^n(\theta_n)\right)}_{\text{OCV difference}} + \underbrace{\left(\eta_p - \eta_n\right)}_{\text{reaction overpotentials}} + \underbrace{\Delta\phi_e}_{\text{electrolyte concentration term}} - \underbrace{I\left(R_{\mathrm{ohm}} + R_{\mathrm{el}} + R_{\mathrm{film}}\right)}_{\text{ohmic \& film drops}}, \tag{6}$$

Where $V_{cell}$ was the output, and $I$ was the input. Often, the surface stoichiometries are normalized to help with numerical conditioning:

$$\theta_n = \frac{c^n_{\mathrm{s,ss}}}{c^n_{\mathrm{s,max}}}, \qquad \theta_p = \frac{c^p_{\mathrm{s,ss}}}{c^p_{\mathrm{s,max}}},$$

The reaction overpotentials were modelled as (Moura et al, 2017)

$$\eta_k = \frac{2RT}{F}\,\mathrm{arcsinh}\left(\frac{I}{2\,I_{0,k}}\right), \qquad k \in \{n, p\},$$

The electrolyte concentration overpotential is modelled as (Moura et al, 2017)

$$\Delta\phi_e = \frac{2RT}{F}\,(1 - t^0_+)\,k_f\,\ln\left(\frac{c_{\mathrm{eright}}}{c_{\mathrm{eleft}}}\right),$$

The effective electrolyte resistance was modeled as:

$$R_{\mathrm{el}} = \frac{1}{2A}\left(\frac{L_n}{\kappa_{n,\mathrm{eff}}} + \frac{2L_{\mathrm{sep}}}{\kappa_{s,\mathrm{eff}}} + \frac{L_p}{\kappa_{p,\mathrm{eff}}}\right),$$

This was a control-oriented lumping consistent with expressing electrolyte ohmic losses as an effective resistance term within the voltage decomposition (Moura et al, 2017).

This concludes the presentation of the SPMe representation of a lithium-ion battery. The usual SPMe representation was transformed into a state-space representation using spatial discretization. The main insights that were obtained from this derivation are:

- A lithium-ion battery can be represented as a linear dynamic block followed by nonlinearity. The state update equation was linear (in $x$ and $I$)., whereas the output equation is nonlinear (in $x$ and $I$).
- The dynamics are only a function of the diffusion coefficient of the electrolyte. This is a key observation meaning that the poles of an estimated transfer function are only a function of the diffusion coefficient of the electrolyte.

To validate and test the model, it fits experimental data. The nonlinearity of the output equation was approximated using a polynomial. The optimization problem to find the best model was

$$minimize\ \frac{1}{N}\sum_{k=0}^{N-1} |\, y_k - g(x_k, u_k, \theta)|_2^2$$

$$\text{subject to } x_{k+1} = f(x_k, u_k, \theta), k = 0,1, \dots, N-1$$

The data consisted of 25 charge/discharge cycles from a lithium-ion battery with composite solid polymer electrolytes (CPSEs), specifically, electrolytes with a distribution of TEMPO-oxidized cellulose nanofibrils (t-CNFs) of poly(ethylene oxide) (PEO). The results are shown in Figures 8 and 9 respectively.

In Figure 8, one discharge cycle is shown and the SPMe model fits the data very well. Different orders of polynomials were tested, and it was determined that a 17$^{th}$ order polynomial has the best fit.

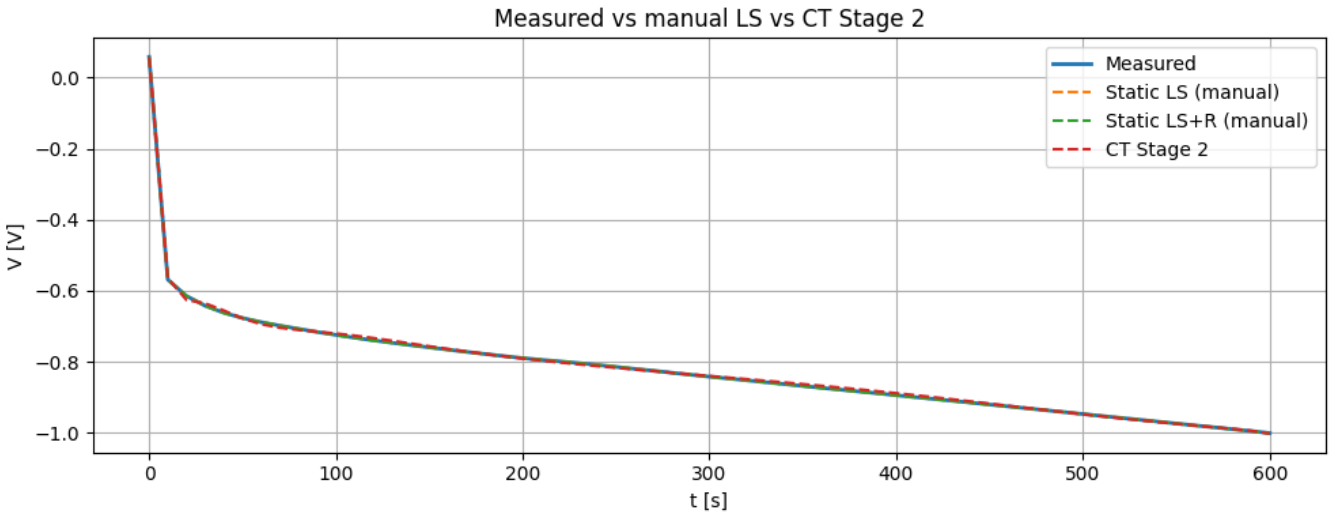



*Figure 8. Fit of SPMe model to experimental data*

The model was fitted to the 25 charge and discharge cycles with the root mean square error (RMSE) being 0.014 $\pm$0.0034 V. From the SPMe model, it was possible to obtain an estimate of certain physical parameters, for example, the effective resistance of the battery $R_0 = R_\Omega + R_{el} + R_{film}$ could be estimated. In Figure 9, the estimated $R_0$ was plotted for each of the 25 charge/discharge cycles.

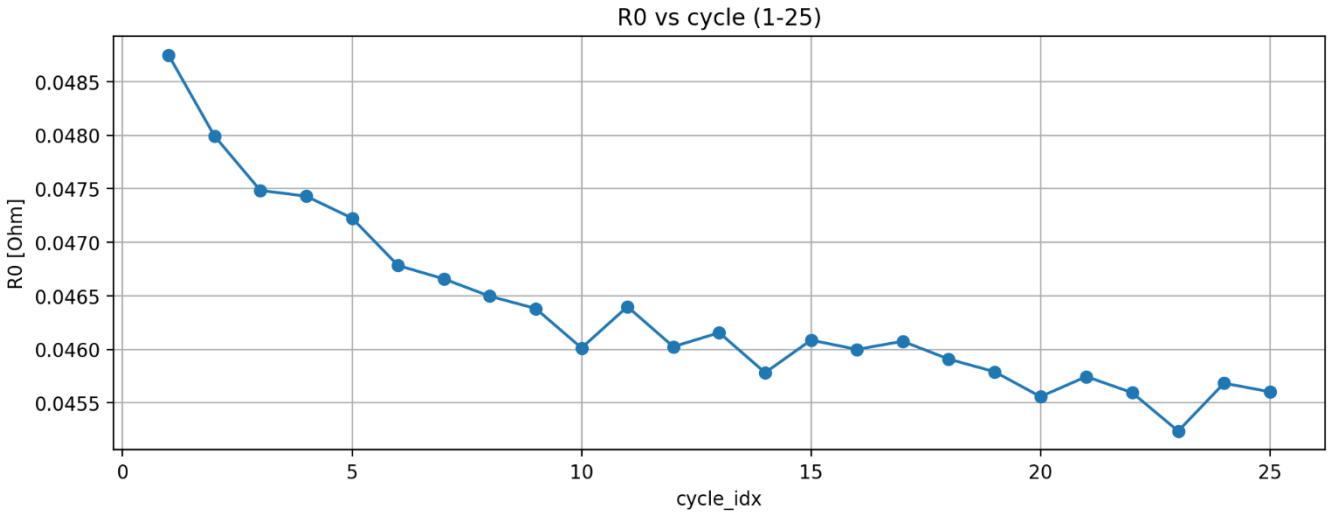



*Figure 9. Estimated $R0$ for each charge/discharge cycle.*

From Figure 9 a trend is evident and indicative of changes in the battery dynamics over time. To further validate the results, further experimental testing is required, including data from where the battery is charged/discharged but periodically during the cycle testing, and certain parameters of the battery are experimentally determined. Currently, the curve in Figure 9 appears to be indicative of dendrite formation, with battery resistance decreasing.

### Milestone 2

The main objective in milestone 2 is to develop a modular network model of a microgrid. This is a critical development to achieve the overall project objective of being able to monitor a battery while it is connected and operating in a grid. The microgrid that will be modelled in this report consists of a battery, inverter, and load.

In this section a comprehensive grid connected power system (GCPS) modeling and identification framework wad proposed that explicitly embedded the battery, capturing the interactions with surrounding power-electronic subsystems under load and operating-condition variations. The GCPS was formulated in an Input-State-Output (ISO) port-Hamiltonian (PH) setting, yielding a parametric and modular-by-construction state-space representation--enabling subsystem augmentation (e.g., DC-DC converters) without re-deriving the full system equations.

The model was built by decomposing the GCPS into three subsystems: the battery, a three-phase inverter with RLC filter, and a connected load. Passive components follow Kirchhoff's laws, while a network-graph topology with primal--dual properties captured the inverter's nonlinear switching in a structure-consistent manner. The integrated port-Hamiltonian (PH) model was validated against a high-fidelity MATLAB/Simulink reference.

*Subsystem Decomposition and Energy-Based Port–Hamiltonian (PH) Framework*

The PH framework represented components as energy storing, dissipating, and interconnection (routing) elements that exchange power through ports. In PH framework, subsystem interconnection was governed by the exchange of flow $f \in F$ and effort $e \in E$ variables, whose product defines the instantaneous power $P = e^{\top} f$.

The interconnection structure was encoded in a Dirac structure $D \subset F \times E$, enforcing power conservation via the flow–effort balance, yielding a differential-algebraic equation (DAE) that admitted modular composition without re-deriving global equations.

This DAE is recast into the ISO PH state-space form:

$$\dot{x} = J(x) - R(x)\nabla H(x) + G(x)\,u, y = G\top(x)\nabla H(x)$$

where $H(x)$ was the stored energy, $J(x) = -J^{\top}(x)$ was the power-conserving interconnection matrix, and $R(x) \geq 0$ captured dissipation.

For this project, the GCPS was decomposed into three individual subsystems: a battery ($\Sigma_1$), a DC-link and three-phase DC–AC inverter with RLC/LC filter ($\Sigma_2$), and a time-varying grid-connected load ($\Sigma_3$ ) as shown in the right-hand side of Figure 10. For each subsystem an ISO PH–model was derived interconnected as shown in the left-hand side of Figure 10.

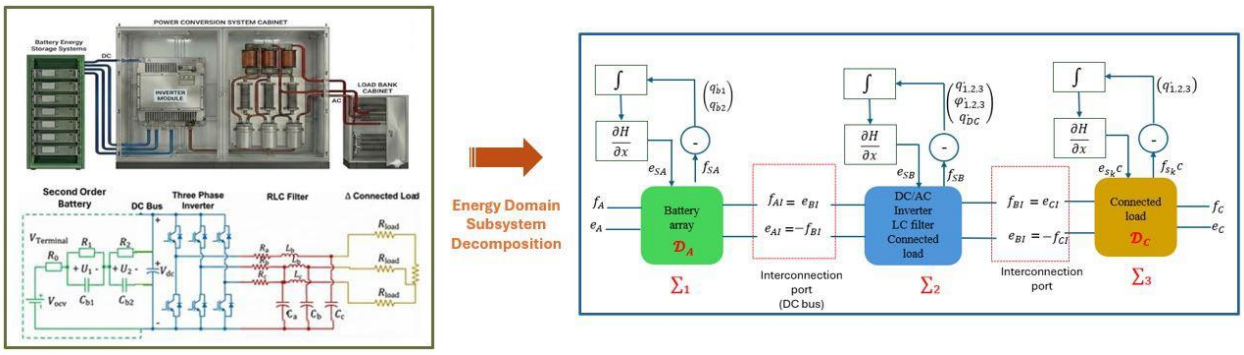



*Figure 10. GCPS consisting of three components, a battery, inverter and load.*

For the linear subsystems, battery ($\Sigma_1$) and load ($\Sigma_3$), the ISO–PH formulation followed directly from Kirchhoff's laws (KVL/KCL). For the battery, the ISO form is represented as:

$$\begin{bmatrix}\dot{q}_{b1}\\ \dot{q}_{b2}\end{bmatrix} = -\begin{bmatrix}\frac{R_0+R_1}{R_0R_1} & \frac{1}{R_0}\\ \frac{1}{R_0} & \frac{R_0+R_2}{R_0R_2}\end{bmatrix}\begin{bmatrix}\frac{q_{b1}}{C_{1b}}\\ \frac{q_{b2}}{C_{2b}}\end{bmatrix} - \begin{bmatrix}\frac{1}{R_0}\\ \frac{1}{R_0}\end{bmatrix}(v_{\text{term}} + v_{\text{ocv}}), \quad y = \begin{bmatrix}-\frac{1}{R_0} & -\frac{1}{R_0}\end{bmatrix}\begin{bmatrix}\frac{q_{b1}}{C_{1b}}\\ \frac{q_{b2}}{C_{2b}}\end{bmatrix}, \quad H(q_b) = \frac{q_{b1}^2}{2C_{1b}} + \frac{q_{b2}^2}{2C_{2b}}$$

where $R$ and $C$ denote the battery's internal resistances and capacitances.

In the inverter, pulse-width modulation (PWM) switching induced nonlinear, hybrid, time-varying inverter dynamics naturally modeled using DAEs, and addressed a power-preserving Primal–Dual Network-Graph PH formulation. The inverter network consisted of three internal subsystems (DC source, switching legs, and RLC filter), and each was described by associated incidence matrices. These matrices enforced flow continuity (KCL) and effort balance (KVL), ensuring mathematically consistent power-flow accounting across interconnections.

PWM switching was captured via Virtual Element Modeling (VEM) with a defined static reference graph (all switches open), and each switching mode applied as a linear transformation to generate mode-dependent flow/effort incidence matrices that exactly encoded the switch states, avoiding linearized switch approximations. These were concatenated in the Dirac structure (DAE) to convert into a compact PH–ISO of $\Sigma_2$:

$$\dot{x} = \left(\underbrace{\begin{bmatrix}\mathbf{0}_{3\times3} & -\mathbf{I}_{3\times3}\\ \mathbf{I}_{3\times3} & \mathbf{0}_{3\times3}\end{bmatrix}}_{J} - \underbrace{\begin{bmatrix}\mathbf{0}_{3\times3} & \mathbf{0}_{3\times3}\\ \mathbf{0}_{3\times3} & \operatorname{diag}(-R_a,-R_b,-R_c)\end{bmatrix}}_{R}\right)\frac{\partial H}{\partial x}(x) + \underbrace{\begin{bmatrix}\mathbf{0}_{3\times2}\\ g_{dc}(S) \quad g_{ac}\end{bmatrix}}_{G(S)}\begin{bmatrix}u_{dc}\\ u_{ac}\end{bmatrix}, \quad g_{dc}(S) = \begin{bmatrix}\frac{2}{3}s_a - \frac{1}{3}s_b - \frac{1}{3}s_c\\ \frac{2}{3}s_b - \frac{1}{3}s_a - \frac{1}{3}s_c\\ \frac{2}{3}s_c - \frac{1}{3}s_a - \frac{1}{3}s_b\end{bmatrix}, \quad g_{ac}^{\top} = \begin{bmatrix}1 & -1 & 0\\ 0 & 1 & -1\\ -1 & 0 & 1\end{bmatrix},$$

$$y_{dc} = -\begin{bmatrix}\mathbf{0}_{1\times3} & g_{dc}^{\top}(S)\end{bmatrix}\frac{\partial H}{\partial x}(x), \qquad y_{ac} = g_{ac}^{\top}(S)\frac{\partial H}{\partial x}(x).$$

The individual subsystem ISO models ($\Sigma_1$, $\Sigma_2$ and $\Sigma_3$) are interconnected by concatenating states/inputs. The total stored energy consists of the sum of subsystem energies.

The global matrices ($J_c$, $R_c$, $G_c$) were assembled in block form from the local matrices and coupled via the power-conserving Dirac structure, yielding a unified high-fidelity PH–ISO model for the full conversion chain (battery, DC-link, switching inverter, and load). The modular-by-construction ISO–PH model of the GCPS included:

$$\dot{x} = \mathcal{J}\nabla H(x) + \underbrace{\gamma(S)\,(u_{dc} + v_{ocv})}_{\text{DC input}} + \underbrace{g_{AC}(S)\,u_{AC}}_{\text{AC input}}, \quad y_{dc} = -\begin{bmatrix}-\frac{1}{R_0} & -\frac{1}{R_0} & \mathbf{0}_{1\times2} & g_{dc}^{\top}(S)\end{bmatrix}\nabla H(x), \quad y_{ac} = g_{ac}^{\top}(S)\,\nabla H(x),$$

$$\dot{x} = \left[\dot{q}_{b1},\ \dot{q}_{b2},\ \dot{q}_{dc},\ \dot{q}_a,\ \dot{q}_b,\ \dot{q}_c,\ \dot{\varphi}_a,\ \dot{\varphi}_b,\ \dot{\varphi}_c\right]^{\top}, \quad \nabla H(x) = \left[\frac{q_{b1}}{C_{b1}},\ \frac{q_{b2}}{C_{b2}},\ \frac{q_{dc}}{C_{dc}},\ \frac{q_a}{C_a},\ \frac{q_b}{C_b},\ \frac{q_c}{C_c},\ \frac{\varphi_a}{L_a},\ \frac{\varphi_b}{L_b},\ \frac{\varphi_c}{L_c}\right]^{\top},$$

$$\mathcal{J} = J - R \triangleq \begin{bmatrix}A & \mathbf{0}_{3\times3} & B\\ \mathbf{0}_{3\times3} & C & D\\ \mathbf{0}_{3\times3} & E & F\end{bmatrix}, \ A = \begin{bmatrix}-\frac{R_0+R_1}{R_0R_1C_{b1}} & -\frac{1}{R_0} & 0\\ -\frac{1}{R_0} & -\frac{R_0+R_2}{R_0R_2C_{b2}} & 0\\ \frac{1}{R_0} & \frac{1}{R_0} & -\frac{1}{R_0}\end{bmatrix}, \ B = \begin{bmatrix}0 & 0 & 0\\ 0 & 0 & 0\\ -s_a & -s_b & -s_c\end{bmatrix}, \ C = \frac{1}{R_{\text{load}}}\begin{bmatrix}-2 & 1 & 1\\ 1 & -2 & 1\\ 1 & 1 & -2\end{bmatrix}$$

$$D = -\mathbf{I}_3,\ E = \mathbf{I}_3,\ F = -\operatorname{diag}(R_a,R_b,R_c),\ \gamma(S) = \left[-\tfrac{1}{R_0},\ -\tfrac{1}{R_0},\ \mathbf{0}_{2\times1},\ g_{dc}(S)\right]^{\top}.$$

The objective in this project was to estimate the battery dynamics given voltage and current measurements at the terminals of the battery. Because of the structure of the network, it was possible to isolate the battery dynamics in a transfer function model. This is done through *model immersion,* as shown in Fig.11, partitioning the global system into two interacting components: $\Sigma_1$ and $\bar{\Sigma} \triangleq (\Sigma_2, \Sigma_3)$. This immersion removed unmeasured internal variables from the identification model while preserving the exact input–output dynamics between the measured terminal variables, $v_{\text{bat}}$ and $i_{\text{bat}}$, without changing their dynamics.

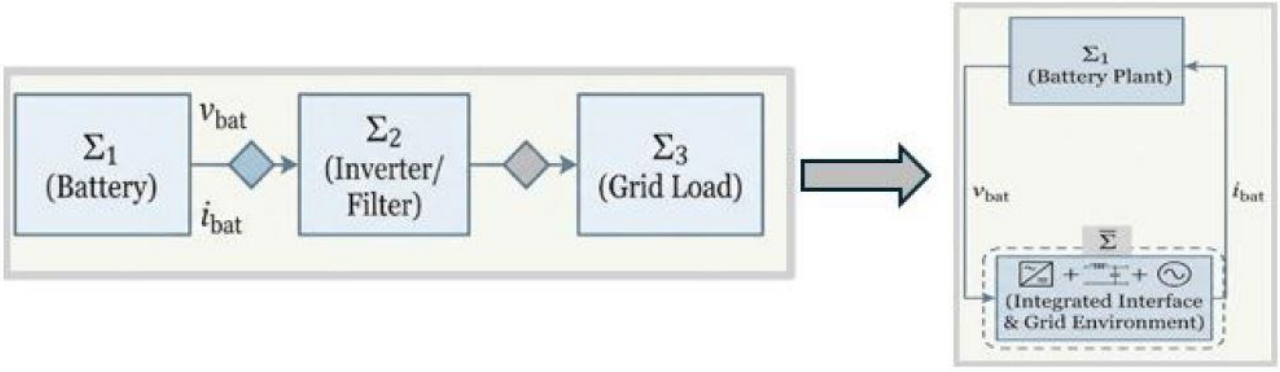



*Figure 11. Immersion of GCPS to isolate the battery dynamics.*

The resulting interconnection, as shown in Fig. 11, between $\Sigma_1$ and $\bar{\Sigma}$ constituted a classical closed-loop identification problem, where $v_{bat}$ and $i_{bat}$ were measured, and the objective was to estimate a transfer function that represents $\Sigma_1$. In this case, the Direct Method, resulting in the lowest variance estimate (Ljung, 1999), meaning the noise needed to be properly modelled and a Box-Jenkins models structure used. The one-step ahead prediction for the Box-Jenkins model structure is (Ljung, 1999):

$$\hat{y}(t|t-1,\theta) = H^{-1}(q,\theta)G(q,\theta)u(t) + \big(1 - H^{-1}(q,\theta)\big)y(t)$$

where $y$ was the output (terminal voltage $v_{bat}$), $u$ was the input (terminal current, $i_{bat}$), $q$ was the shift operator such that $q^{-1}u(t) = u(t-1)$, $G(\theta)$ was the transfer function representing the battery dynamics (the ECM), $H(\theta)$ was a transfer function representing the noise model (to model disturbances affecting the system) and $\theta$ was a parameter vector representing the unknown parameters of $G$ and $H$. Specifically:

$$G(q,\theta) = \frac{b_0 + b_{1q}^{-1} + \cdots + b_{n_b}q^{-n_b}}{1 + a_1 q^{-1} + \cdots + a_{n_a}q^{-n_a}},$$

$$H(q,\theta) = \frac{c_0 + c_{1q}^{-1} + \cdots + c_{n_c}q^{-n_c}}{1 + d_1 q^{-1} + \cdots + d_{n_d}q^{-n_d}},$$

where $n_a, n_b, n_c$ and $n_d$ were the model orders, with a selected priori and $\theta = [b_0 \cdots b_{n_b}\ a_1 \cdots a_{n_a}\ c_0 \cdots c_{n_c}\ d_1 \cdots d_{n_d}]$ being the unknown parameters estimated from the data.

The objective function used to estimate the parameters from data was the sum of squared prediction errors:

$$V(\theta) = \sum_{t=0}^{N-1} \left(y(t) - \hat{y}(t|t-1,\theta)\right)^2$$

where $y(k)$ was the measured output, and $\hat{y}$(k) was the one step ahead prediction of $y(k)$. The prediction error is denoted as:

$$\varepsilon(t,\theta) = y(t) - \hat{y}(t|t-1,\theta).$$

***Model Testing***

The residual tests were used for model validation, to determine whether the dynamics of the data battery system were fully captured and consistent with standard practices per the system identification literature (Ljung, 1999).

There were two residual tests which, cross-correlated to zero between the input and the autocorrelation of the prediction error for all lags greater than zero. This was indicative an unpredictable variable assumed to be white noise in this case.

The main interpretation of the residual tests was used to confirm/check whether all information has been captured by the model. For example, if there were a correlation between the input and the prediction error, it meant that the model did not capture all dynamics present in the data driven by the input. The residual tests were directly assessed for model fitness using a 95% confidence interval evaluation and assuming inequities are satisfied.

The first inequality check assessed was evaluated using (Ljung, 1999):

$$|R_{\varepsilon u}(\tau)| < \sqrt{\frac{P}{N}} N_\alpha, \text{ for all } \tau$$

where

$$P = \sum_{\tau=\infty}^{\infty} R_\varepsilon(\tau) R_u(\tau)$$

and $N_\alpha$ was determined by the 95% confidence interval and $N$ was the data length.

The second inequality check assessed for autocorrelation 95% interval confidence:

$$\left|\frac{R_\varepsilon(\tau)}{R_\varepsilon(0)}\right| < \sqrt{\frac{1}{N}} N_\alpha \text{ for all } \tau > 0.$$

The proposed algorithm, using the Direct Method of closed loop identification to estimate battery dynamics, was validated using simulated data. The simulated data was generated using a high-fidelity MATLAB/Simscape benchmark model.

The proposed Matlab/Simscape model was simulated over $T_{\text{sim}}$ = 100 s with a sampling rate of $T_s = 6.667 \times 10^{-4}$ capturing both high-frequency switching transients as well as slower battery discharge dynamics.

The parameters used in the simulation are shown in Table 8. The battery was initialized at full charge ($u_{ocv}$ = 200) and discharged through a grid-tied SPWM inverter. The DC-side terminal voltage and current were saved.

| Battery Parameters (2-RC Model) | | | | | | Inverter & Grid | | | | | |
|---|---|---|---|---|---|---|---|---|---|---|---|
| **Par.** | **Sym.** | **Val.** | **Par.** | **Sym.** | **Val.** | **Par.** | **Sym.** | **Val.** | **Par.** | **Sym.** | **Val.** |
| Ohmic res. | $R_0$ | 10 mΩ | Load res. | $R_{load}$ | 75.0 Ω | DC-link cap. | $C_{dc}$ | 2.0 mF | Filter cap. | $C_f$ | 8.0 $\mu$F |
| Polar. res. | $R_1 = R_2$ | 1.0 Ω | Polar. cap. | $C_{b1} = C_{b2}$ | 20.0 F | Filter ind. | $L_f$ | 2.0 mH | Filter res. | $R_L$ | 1.0 nΩ |

*Table 8. System Parameters Used in Simulation*

The actual battery dynamics were captured by the transfer function:

$$G(z) = \frac{-0.1z^2 + 0.11z + 0.009}{z^2 - 1.99z + 0.99}$$

Using the methodology described above, the estimated transfer function was calculated as:

$$G(z) = \frac{-0.113z^2 + 0.095z}{z^2 - 1.92z + 0.93}.$$

The estimated transfer function was close to the transfer function of the simulated battery, and the estimated model was validated using the residual tests described above. The model passes both residual tests as shown in Figure 12, with results within 95% confidence interval: capturing the dynamics of the data generating system.

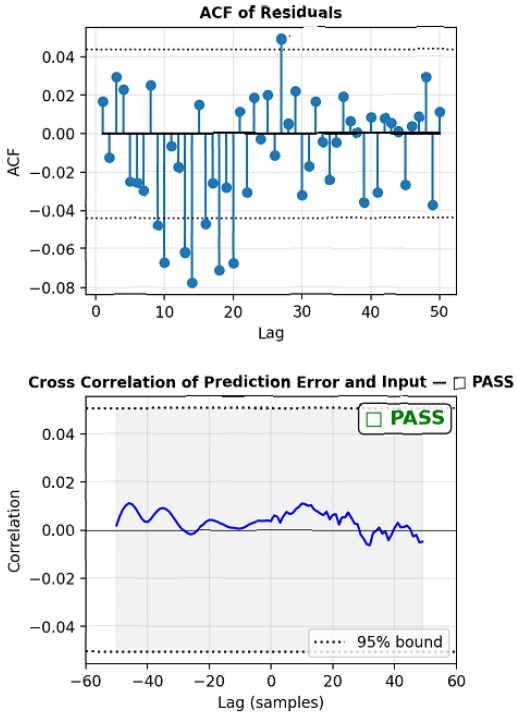



*Figure 12. Results of residual test using simulated data.*

Predictive battery voltage was assed using the model and was compared with the actual output as shown on Figure 13.

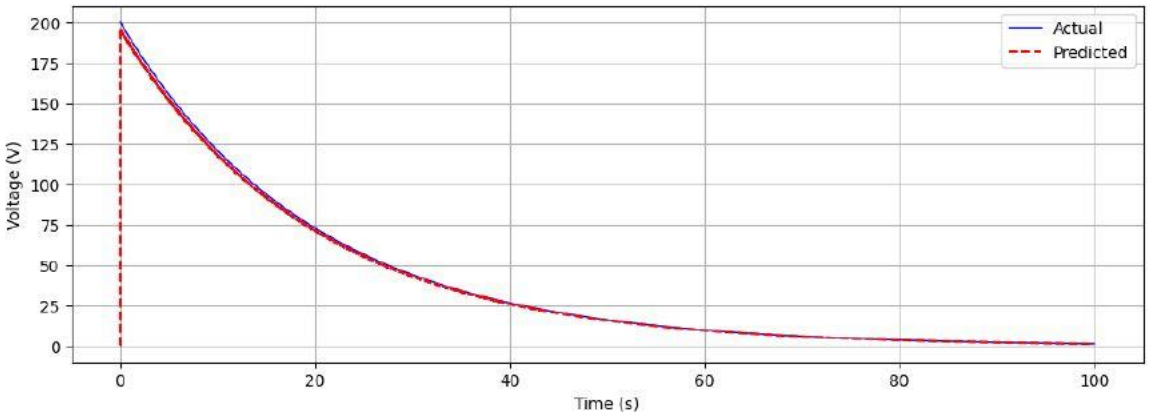



*Figure 13. One step ahead prediction of voltage using model and actual voltage compared.*

The graph illustrates a strong relationship between estimated and measured voltages with a prediction error of approximately 4%. Thereby, demonstrating that developed algorithm was able to estimate the battery dynamics from simulated data

**Milestone 3**

In this phase of work, the algorithm was implemented on data collected from a vanadium redox flow battery installation for testing and limited validation.

***Data Set***

The data set used from the utility-scaled integrated grid consisted of 112 days of cycling between charging and discharging, with voltage and current measurements recorded on the battery terminals every minute.

The vanadium redox battery associated with the utility-scale operational grid was not connected to the Alberta Interconnected Electric System during time of data collection though it was connected to power electronics (including a battery management system) and a load. This set up closely resembled the setup of the developed simulator apart from the presence of a feedback controller between the load voltage and the inverter on the utility-scaled operation. This difference did not impact the battery model materially, and in the immersed network, the controller was absorbed into the model of the feedback path from $v_{bat}$ to $i_{bat}$, with the battery dynamics remaining isolated in the model.

***Algorithm Design***

The algorithm developed in association with this Work Area was used to monitor physical properties of a vanadium redox flow battery with the algorithm estimating an equivalent circuit model (ECM) from the data. The parameters of the ECM model depend on physical characteristics of the battery, with mapping from ECM to physical characteristics completed as part of Milestone 1 activities for a lithium-ion battery.

This algorithm was applied to a system with a vanadium redox flow battery, rather than the originally planned lithium-ion battery, to allow for the model to be tested using the operating data for the utility-scaled grid operation. As a result, the interpretation of the estimated ECM was expected to differ due to associated differences battery chemistry physics.

Experimental validated mapping from ECM to the physics of a vanadium redox flow battery could not be undertaken in the time allotted for the project scope, therefore published data was used (Yesilyurt et. al 2023, Derr et. al. 2017). The studies referenced determined that the poles of the ECM model were directly related to the charge transfer resistance. The charge transfer resistance is significant as it relates to degradation as the chemical reactions on the half-cells prompt decays on the structure of the porous electrodes, thereby causing an increase in resistance to electron flow over time (Yesilyurt et. al 2023, Derr et. al. 2017).

Changes in the ECM of a vanadium redox flow battery were estimated from data collected from the utility grid physical vanadium redox flow battery data set, with the estimated ECM interpreted using the results of the published data set.

The raw voltage and current data are shown in Figs. 14 and 15.

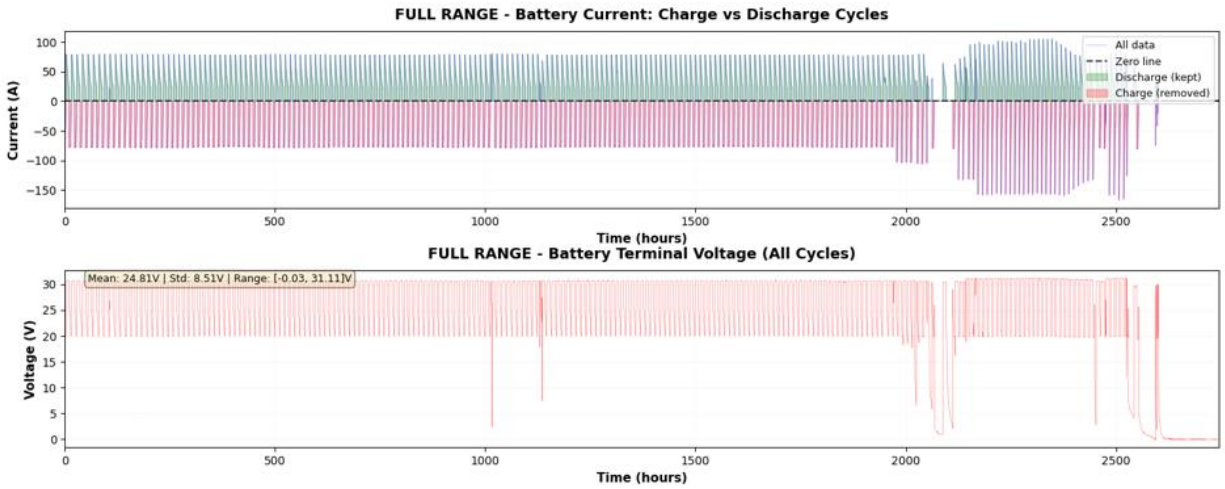



*Figure 14. Voltage and current data from battery installation.*

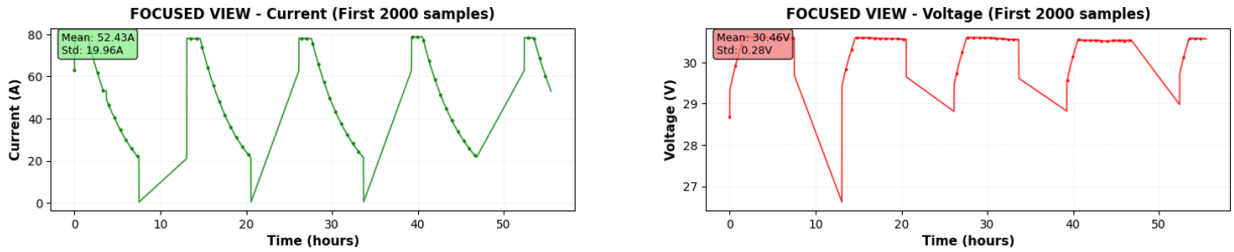



*Figure 15. Zoomed in view of the voltage and current data.*

For the monitoring algorithm, data was split into blocks consisting of five-day intervals, in an attempt to balance sufficient data from an estimation standpoint, and sufficient time to detect relevant battery dynamics. For each block, the dynamics of the battery were estimated with the methodology used to estimate the dynamics of the battery provided below.

The PH model developed in Milestone 2 determined that the battery dynamics could be estimated from the battery terminal voltage and current with the transfer function for the battery contained within a closed loop in the model.

The methodology to estimate the battery dynamics included:

1. Splitting data into time blocks
2. For each segment:
    a. Select $n_a = 2$, $n_b = 2$ with the order of the battery dynamics determined from physical modelling
    b. Select $n_c = 1, n_d = 1$
    c. Determine $\theta$ that minimizes the sum of squared prediction errors (V).
    d. Assess the results of the residual testing
        a. If no pass achieved, increase $n_c$ and $n_d$ by 1 and return to step c.
        b. If pass was achieved, continue to step e.
    e. Return to step 1.

***Algorithm Testing***

For this project there were 23 blocks of data, which were subjected to the close-loop testing method, and represent the battery dynamics as a progression through time. The poles of each of the estimated ECMs were calculated using the published data set, with the poles of the ECM proportional to the charge transfer resistance. Gradual changes to the charge transfer resistance over time were tracked using this algorithm while the battery is in operation.

The validation results of the 23rd data block are shown in Fig 16.

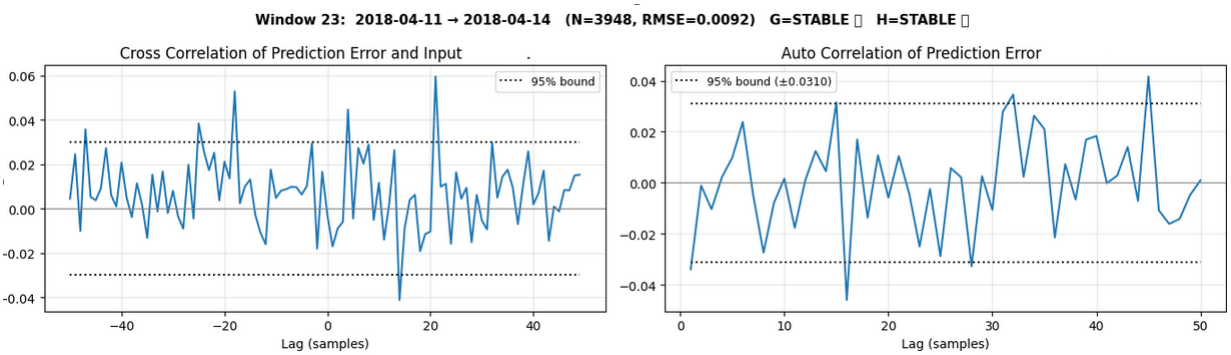



*Figure 16. Validation test for correctness of model with data set #23.*

The majority of the battery dynamics residual tests fell within the 95% confidence interval, apart from a minimal number of data outliers. Additionally, the root mean squared prediction error was 0.0092 and indicative of good model fitness.

The absolute value of the poles for the full set of data blocks is tested are presented in Fig. 17 with the root mean squared prediction error for each data block is shown in Fig 18. The figures illustrate the fitness of the data for all time blocks, even with a limited evaluation sample size., with relatively little variance observed.

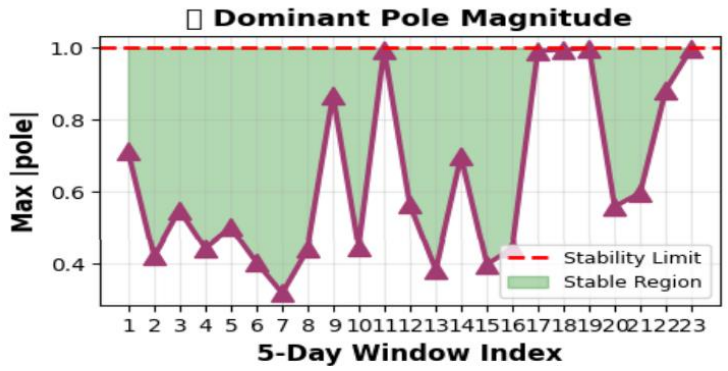



*Figure 17. Max absolute value of estimated poles for each block of data.*

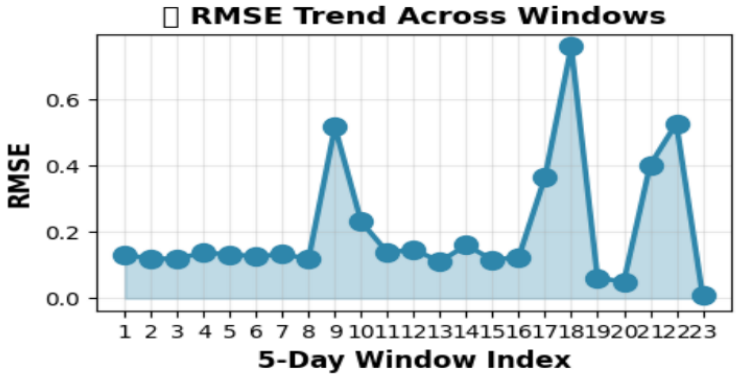



*Figure 18 Root mean squared prediction error for each data block.*

The monitoring algorithm developed for this Work Area has been implemented on a limited set of real data to monitor changes in the physics of a battery while it is in operation, tracking changes to the charge transfer resistance.

**Work Area C – Material selection based on the energy storage device physics**

The updated objective for this section included the development of foundational model that is property-agnostic, enabling future extension to additional electrolyte properties and ultimately connecting to device-level performance.

The following sections describe progress at the material scale, specifically, the development and partially validated machine learning model for predicting ionic conductivity of solid polymer electrolytes (SPEs). The three scales and how they converge are described in detail in the Multi-Scale Integration section highlighted in the Project Results section of this report.

**Milestone 1**

***Model Selection***

To represent the lithium-ion battery, the Doyle-Fuller-Newman was selected. In this model, the governing equations describe mass diffusion within the electrodes and electrolyte, charge balance in both phases, and the reaction kinetics at the electrode–electrolyte interface (represented by the Butler–Volmer equation).

The principal rational selecting this model is that allows for the integration of other degradation modes, allowing for other modeled degradation elements to be easily integrated in future work.

***Sensitivity Analysis***

The sensitivity of material design parameters was influenced via a literature review.

The primary source for the literature review included a study completed by Bradford et al. (2023) which compiled the largest currently available curated dataset of solid polymer electrolyte (SPE) ionic conductivity measurements from the published experimental literature (ACS Central Science, 2023).

The dataset encompasses 3,195 formulations derived from 247 polymer chemistries and 81 lithium salts, extracted from 217 independent publications. There was a total of approximately 8,000 data points; 90% were used to train the model and the remaining 10% were used as the held-out test set.

Each entry provides the polymer SMILES string, molecular weight, lithium salt identity and EO:Li molar ratio, measurement temperature, and conductivity in log S/cm. Because these data originate from multiple independent laboratories using different synthesis procedures and measurement protocols, the dataset reflects realistic variability typical of polymer electrolyte research.

Based on the review findings, the principal modes of degradation identified for SPE based lithium-ion batteries included:

- SEI (solid electrolyte interface) formation
- Lithium (Li) plating
- Electrolyte degradation
- Particle cracking
- Lithium dendrite formation and penetration
- Electrode – electrolyte interface degradation
- Loss of ionic conductivity due to morphological changes in polymers

Though some preliminary simulation experiments were conducted on other identified degradation considerations, conductance was the parameter primarily targeted for modeling and testing. This parameter represents the most fundamental transport property governing the operational feasibility of solid polymer electrolytes.

The room-temperature ionic conductivity of most polymer electrolytes is typically below $10^{-5}$ S/cm, which results in high internal resistance and severely limits power capability. As a result, insufficient conductivity remains the primary physical bottleneck preventing widespread replacement of liquid electrolytes with solid polymer systems.

From a modeling standpoint, ionic conductivity also provides the most suitable entry point for validating the proposed machine learning framework. Among the relevant electrolyte properties, conductivity benefits from the largest available datasets, both from curated experimental literature and from high-throughput molecular dynamics simulations. These datasets provide sufficient data density to allow robust training and quantitative benchmarking of the predictive framework.

In contrast, other key parameters such as lithium-ion transference number or mechanical moduli are reported far less frequently in the literature, so there is a lack of datasets of comparable scale and consistency. Young's modulus and mechanical strength data for SPEs are particularly scarce: these measurements are rarely reported alongside conductivity in the same publication, and the experimental protocols for measuring them are even less standardized than those used for EIS-based conductivity. As a result, building a robust predictive model for mechanical properties would require substantially more dedicated experimental work before the data density would support reliable training.

***Milestone 2***

Tasks started in Milestone 1 for this Work Area continued in Milestone 2 with the addition of work associated with on designing the data generation pipeline needed to train and validate models.

***Design data synthesis for framework***

Polymer materials have limited conductivity, and this was a key consideration for degradation potential and electron movement challenges nanoparticles are added to the electrolyte to boost the overall conductivity, resulting in a better battery. These material properties are governed by the following variables:

Considerations to include nanoparticles as factors for improving polymer conductance were explored in Milestone 2 including considerations such as:

- Size of polymer molecules
- Size of nanoparticles
- Polymer-nanoparticle interaction energy
- Nanoparticle-nanoparticle interaction energy
- Nanoparticle loading

These variables were ultimately included in the model design to estimate the conductivity of resulting electrolytes. A total of 152 new lithium conductors were identified that demonstrated evidence of high ionic conductance and were flagged for further testing and evaluation.

Several neural network architectures were evaluated for use. A Siamese-style model (Fig. 19) was evaluated due to its ability to create pairings form unlabeled data in published data sets. With only 112 labeled data points and nearly 5000 unlabeled data points in the Bradford et al. dataset, a need existed to leverage all available date for model construction.

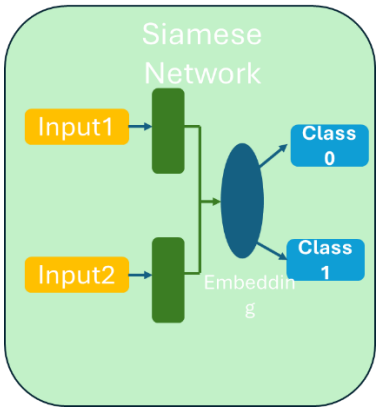



*Figure 19. Illustration of the structure of a Siamese Network*

Dendrite formation and suppression are identified as a key engineering challenge for solid polymer electrolytes, however the current ML framework does not yet predict dendrite-related failure mechanisms. This is because dendrite suppression depends on mechanical modulus, interfacial stability, and morphological factors that are not currently encoded in the model inputs. This capability is identified as a priority for future development, pending availability of suitable training data.

**Milestone 3**

Work in this Milestone mainly consisted of constructing battery cells and testing the materials model developed on published and physical experiments for preliminary validation efforts.

***Coin Cell Fabrication and Testing Methodology***

To bridge the gap between material-level characterization (ionic conductivity measured via EIS) and device-level performance, SPE films were also assembled into coin cell configurations for electrochemical cycling characterization. Coin cell data represent the intermediate scale linking the property prediction framework to the battery modeling work carried out in parallel by the device team.

The coin cell data serve two roles within the broader framework. First, the ionic conductivity values predicted by the ML model for a given formulation can be used as inputs to an equivalent circuit model of the coin cell, linking predicted transport properties to expected cell-level resistance and rate capability. Second, cycling data, are shared with the battery modeling team to inform device-scale simulations. This creates an explicit data path from molecular composition to cell performance, which is the core connective tissue of the multi-scale framework.

*Cell Assembly*

Coin cells (CR2032 format) were assembled inside an argon-filled glovebox ($H_2O$ and $O_2$ < 0.1 ppm) to prevent moisture exposure. The cell stack consisted of a lithium metal anode, the polymer electrolyte film, and a lithium cobalt oxide (LCO). Stainless steel spacers and wave springs were used to ensure uniform pressure and good contact across the electrolyte membrane. All assembly steps were performed under strictly controlled inert atmosphere conditions.

*Electrochemical Cycling Protocol*

Assembled coin cells were subjected to galvanostatic charge–discharge cycling on a BioLogic battery cycler. Cells were conditioned at C/20 for the first three cycles to establish stable interfacial contact between the polymer electrolyte and the lithium anode. Subsequent cycling was conducted at C/10 over

a defined voltage window. Capacity retention and Coulombic efficiency were monitored as a function of cycle number.

In addition, electrochemical impedance spectroscopy (EIS) was performed on selected coin cell configurations at defined cycle intervals to track interfacial resistance evolution. This allows the connecting of bulk conductivity predictions (from the ML model) to changes in interfacial resistance observed during cycling, providing a quantitative bridge between material-scale properties and device-scale performance.

***Computational Architecture***

The predictive framework was designed to leverage large-scale chemical representation learning while remaining robust to the limited size of experimentally available SPE datasets. Rather than training a model from scratch, the approach borrows a deep understanding of molecular chemistry that already exists — from a pretrained foundation model — and directs it toward a specific prediction task.

Polymer repeat units were represented using SMILES strings, a standardized encoding of molecular connectivity widely used in chemical databases and machine learning pipelines. Molecular structures were then embedded using the SMI-TED transformer model developed by IBM Research, which was pretrained on approximately 91 million molecular structures using self-supervised learning and produces a 384-dimensional latent embedding capturing structural and functional relationships across chemical space. SMI-TED operates on the same principle as large language models: just as a language model learns patterns of human language from billions of sentences, SMI-TED learned patterns of molecular chemistry from 91 million molecular structures.

The encoder weights were intentionally kept frozen during model training. The experimentally available SPE datasets contain only a few thousand labeled measurements, which is insufficient to reliably fine-tune a model with hundreds of millions of parameters without severe overfitting. Treating the pretrained model as a fixed chemical feature extractor allows the framework to preserve the chemical knowledge learned during large-scale pretraining while ensuring stable training on comparatively small electrolyte datasets.

Because ionic conductivity in polymer electrolytes depends not only on molecular chemistry but also on thermodynamic and compositional variables, the molecular embedding was augmented with experimentally relevant descriptors including polymer molecular weight, salt concentration, and measurement temperature. The combined feature vector was then passed to a regularized feed-forward neural network trained to predict ionic conductivity expressed as $\log_{10}(\sigma)$.

This architecture intentionally separates molecular representation learning from property prediction. Because the molecular encoder is fixed and makes no assumptions about which property is being predicted, entirely new properties can be added by training a separate prediction layer on the same embeddings, without retraining or modifying the underlying chemistry model. The framework is therefore a platform for multi-property SPE screening, not a single-purpose tool. Future work will extend this to transference number, electrochemical stability window, and — as data availability allows — mechanical moduli.

In the present work, the SMI-TED model was applied for the first time to the prediction of transport properties in polymer electrolytes.

***Datasets***

A central challenge in materials informatics is the conversion of discrete chemical structures into continuous numerical representations that can be used in machine learning models. To rigorously evaluate the predictive capability of the framework, three independent datasets were employed, representing distinct sources of ionic conductivity data with different levels of experimental control and data variability. These datasets were intentionally treated as separate validation domains throughout the study. No cross-contamination between datasets was permitted during training or evaluation, to ensure an unbiased assessment of model generalization across different data regimes.

*Bradford et al. (2023) — Experimental Literature Dataset*

Bradford et al. compiled the largest currently available curated dataset of solid polymer electrolyte (SPE) ionic conductivity measurements from the published experimental literature (ACS Central Science, 2023). The dataset encompasses 3,195 formulations derived from 247 polymer chemistries and 81 lithium salts, extracted from 217 independent publications. There was a total of approximately 8,000 data points; 90% were used to train the model and the remaining 10% were used as the held-out test set. Each entry provides the polymer SMILES string, molecular weight, lithium salt identity and EO:Li molar ratio, measurement temperature, and conductivity in log S/cm. Because these data originate from multiple independent laboratories using different synthesis procedures and measurement protocols, the dataset reflects realistic variability typical of polymer electrolyte research.

*HTP-MD (2023) — High-Throughput Molecular Dynamics Simulation Dataset*

The HTP-MD dataset was generated by Xie et al. at the Toyota Research Institute and reported in APL Machine Learning (2023). This dataset contains ionic conductivity values obtained from high-throughput molecular dynamics simulations of 5,962 polymer–salt systems, totaling approximately 6,200 data points; 90% were used for training and 10% for testing. Unlike the literature dataset, all simulations were performed using a fully standardized computational protocol including identical force fields, equilibration procedures, and simulation temperatures. This uniformity significantly reduces measurement variability compared to experimental datasets. The internal consistency of the simulation framework makes this dataset substantially lower in noise, providing an important reference domain for evaluating the intrinsic predictive capability of the ML framework under conditions where experimental variability is minimized.

*In-House Experimental Dataset*

For validation on experimental systems synthesized and characterized by our team, polymer electrolyte films were prepared in-house. Poly(ethylene oxide) (PEO) with a molecular weight of 100,000 g/mol was used together with lithium perchlorate ($LiClO_4$) and lithium bis(trifluoromethanesulfonyl)imide (LiTFSI), procured from Sigma-Aldrich and used as received. In all formulations, the ethylene oxide-to-lithium molar ratio (EO:Li) was fixed at 10:1. Deionized water (Milli-Q, 18.2 MΩ·cm) was used as solvent.

SPE films were fabricated by dissolving PEO in DI water, adding the lithium salt, and magnetically stirring for a minimum of 24 hours. Solutions were cast into flat molds and dried in a vacuum oven at 60°C for 48 hours. Films were subsequently stored in an argon-filled glovebox ($H_2O$ and $O_2$ < 0.1 ppm) for at least one week prior to testing.

Ionic conductivity was evaluated by electrochemical impedance spectroscopy (EIS) over a temperature range of 23°C to 65°C using a BioLogic VSP-300 potentiostat with EC-Lab® software. Measurements used

a symmetric two-electrode blocking configuration (electrolyte sandwiched between two stainless steel disk electrodes) with a Teflon spacer to ensure uniform geometry. Impedance spectra were acquired from 0.1 Hz to 3 MHz at an AC perturbation of 10 mV (rms). Bulk ionic resistance was extracted from the high-frequency intercept of the Nyquist plot, and conductivity was calculated as:

$$\sigma\,(\mathrm{S/cm}) \;=\; \mathrm{L} \,/\, (\mathrm{A} \times \mathrm{R})$$

where L is film thickness (cm), A is electrode contact area ($cm^2$), and R is bulk resistance (Ω). Film thickness was measured using a digital micrometer at multiple points and the average used in the calculation. Each film was measured across multiple temperatures, producing a total about 23 data points for validation. These data were never used at any stage of model training — they represent a fully blind out-of-sample test.

| Sample | PEO MW (g/mol) | Li Salt | T (°C) | log σ (S/cm) |
|---|---|---|---|---|
| PEO 4K / $LiClO_4$ | 4,000 | $LiClO_4$ | 23 | -4.57 |
| PEO 4K / $LiClO_4$ | 4,000 | $LiClO_4$ | 35 | -4.41 |
| PEO 4K / $LiClO_4$ | 4,000 | $LiClO_4$ | 45 | -4.06 |
| PEO 4K / $LiClO_4$ | 4,000 | $LiClO_4$ | 55 | -3.73 |
| PEO 4K / $LiClO_4$ | 4,000 | $LiClO_4$ | 65 | -3.46 |
| PEO 100K / $LiClO_4$ | 100,000 | $LiClO_4$ | 23 | -5.01 |
| PEO 100K / $LiClO_4$ | 100,000 | $LiClO_4$ | 30 | -4.61 |
| PEO 100K / $LiClO_4$ | 100,000 | $LiClO_4$ | 35 | -4.43 |
| PEO 100K / $LiClO_4$ | 100,000 | $LiClO_4$ | 45 | -4.12 |
| PEO 100K / $LiClO_4$ | 100,000 | $LiClO_4$ | 55 | -3.8 |
| PEO 100K / $LiClO_4$ | 100,000 | $LiClO_4$ | 65 | -3.53 |
| PEO 1M / $LiClO_4$ | 1,000,000 | $LiClO_4$ | 23 | -5.34 |
| PEO 1M / $LiClO_4$ | 1,000,000 | $LiClO_4$ | 30 | -5.07 |
| PEO 1M / $LiClO_4$ | 1,000,000 | $LiClO_4$ | 35 | -4.87 |
| PEO 1M / $LiClO_4$ | 1,000,000 | $LiClO_4$ | 45 | -4.49 |
| PEO 1M / $LiClO_4$ | 1,000,000 | $LiClO_4$ | 55 | -4.12 |
| PEO 1M / $LiClO_4$ | 1,000,000 | $LiClO_4$ | 65 | -3.82 |
| PEO 1M / LiTFSI | 1,000,000 | LiTFSI | 71.7 | -3.6 |
| PEO 1M / LiTFSI | 1,000,000 | LiTFSI | 60.2 | -3.72 |
| PEO 1M / LiTFSI | 1,000,000 | LiTFSI | 49.4 | -3.98 |
| PEO 1M / LiTFSI | 1,000,000 | LiTFSI | 39.4 | -4 |
| PEO 1M / LiTFSI | 1,000,000 | LiTFSI | 29.9 | -4.62 |
| PEO 1M / LiTFSI | 1,000,000 | LiTFSI | 22.7 | -4.85 |

Table 9. In-House SPE Experimental Data — Ionic Conductivity, polymer molecular weight, system temperature and Composition

***Testing Results***

The results presented below show that the model detects a meaningful structure/conductivity relationship across multiple evaluation domains. However, given the limited size of the in-house experimental dataset and the heterogeneity of the literature data, formal statistical validation is still in progress. These findings should be understood as partially validated model, providing evidence of model capability and guiding ongoing experimental work.

Predictive performance was quantified using Mean Absolute Percentage Error (MAPE). This metric was selected because ionic conductivity spans many orders of magnitude across polymer electrolyte systems, approximately $10^{-10}$ to $10^{-2}$ S/cm in the literature. Performance was evaluated in three sequential steps, each answering a distinct validation question. The framework diagram at the end of this section visually summarizes all three steps and their relationship.

*Step 1 — HTP-MD Simulation Dataset (In-Distribution Accuracy)*

The first evaluation uses the Toyota Research Institute HTP-MD dataset. The model achieved a MAPE of 3.06% on the 596 held-out data points (Figure 20). This strong in-distribution result confirms that the

frozen SMI-TED embeddings, augmented with system descriptors, effectively capture the underlying relationship between polymer chemistry and ion transport when the training data are internally consistent. Because the simulation dataset minimizes experimental variability (all runs use identical protocols and force fields), this result provides an approximate upper bound on the predictive accuracy achievable using the present representation architecture.

No experimental data appears in this step because experimental conductivity and simulated conductivity are not directly comparable — they are produced by fundamentally different processes at different scales with different sources of variability. Mixing them into a single training or test set would obscure the model's actual capabilities rather than reveal them. The purpose of this step is solely to confirm that the molecular embeddings combined with system descriptors successfully capture the structure–conductivity relationship within a controlled, internally consistent dataset.

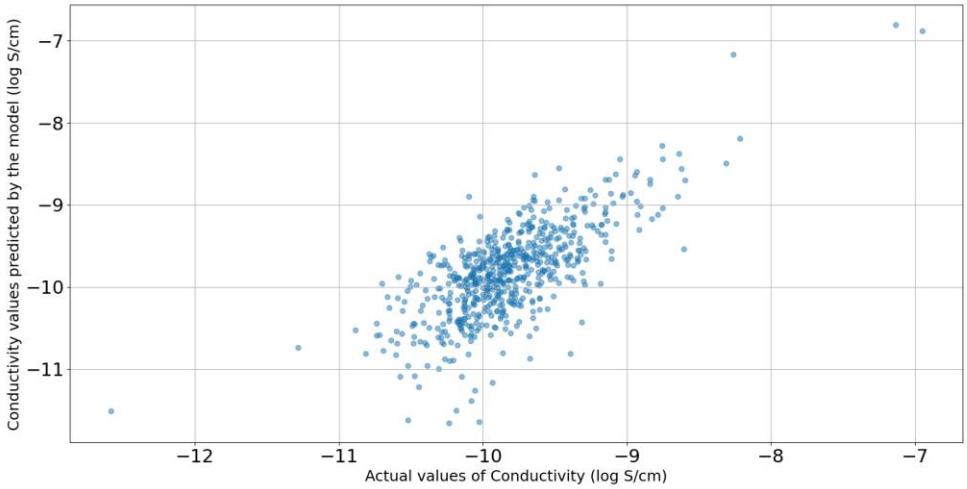



*Figure 20. Predicted vs. actual ionic conductivity for the HTP-MD simulation dataset (held-out test set). MAPE = 3.06%.*

*Step 2 — Bradford et al. (2023) Experimental Dataset (Cross-Distribution Transfer)*

The second evaluation asks whether the structure–conductivity relationship learned from simulation data transfers to real experimental measurements. The Bradford et al. (2023) dataset aggregates approximately 8,000 conductivity measurements from 217 independent publications, spanning a wide range of polymer hosts, lithium salt types, salt concentrations, molecular weights, and measurement temperatures.

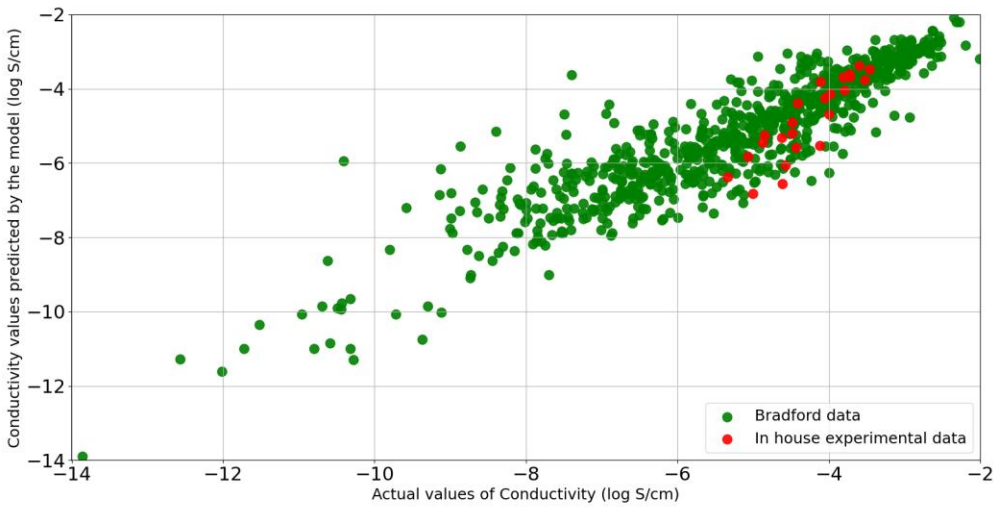



*Figure 21. Predicted vs. actual ionic conductivity for the Bradford literature dataset after manual curation of missing values. Green: literature data; red: in-house EIS measurements (n = 23). MAPE on literature data = 10.3%.*

*Step 3 — In-House Measurements (Direct Out-of-Sample Validation)*

The third evaluation addresses the model's ability to predict conductivity for the PEO-based solid polymer electrolytes synthesized and characterized by this team based on the limited experimental data subset conducted as part of this project. A MAPE of approximately 13% was achieved on 23 out-of-sample measurements that the model and is consistent with the cross-distribution performance observed in Step 2; confirming that the model is generalizing rather than memorizing.

The small dataset size is a constraint of experimental throughput: EIS characterization of a single film batch requires several weeks of synthesis, drying, glovebox storage, and multi-temperature measurement. The current result should therefore be interpreted as a preliminary consistency check, not a definitive validation. As more in-house data points are added, the reliability of this estimate will improve. Data collection is ongoing.

It is also noted that the in-house measured conductivity values tend to be higher than what is predicted by the model for the same formulation. This is at least partly attributable to the historical nature of the training data: the Bradford literature dataset was compiled primarily from older publications in which conductivity values for the same polymer–salt systems are systematically lower than more recent measurements. Over time, researchers have developed better sample preparation techniques, improved glovebox procedures, and more reliable EIS fitting protocols, all of which led to higher reported conductivities for nominally identical materials. Because the model was trained on this older distribution, it under-predicts the conductivities achieved by the improved protocols used in our lab. This is a recognized limitation of the current dataset and is discussed further in the Challenges and Lessons Learned section.

*Comparison with Prior Work*

The conventional approach to property prediction in polymer electrolytes is to build a task-specific model. Bradford et al.'s ChemArr model is a representative example: a graph neural network that embeds the Arrhenius temperature dependence directly into its architecture, trained exclusively on the

Bradford conductivity dataset. ChemArr achieved predictions within 0.5 log S/cm for approximately 49% of polymer species, corresponding to a MAPE of approximately 19%.

The present framework achieves 10.3% MAPE on the same literature corpus while operating under substantially different design constraints. In contrast to ChemArr, which was explicitly engineered for conductivity prediction, the present approach employs a general-purpose molecular foundation model that was not trained specifically for electrolyte systems. The two approaches represent different modeling philosophies: ChemArr prioritizes task-specific accuracy by embedding domain physics directly into the architecture, while the present framework prioritizes architectural generality and transferability, enabling the same molecular representations to be used for predicting multiple electrolyte properties without model redesign.

For the in-house experiments, a MAPE of approximately 13% was achieved on 23 fully blind out-of-sample measurements. This is consistent with the cross-distribution performance seen in Step 2 and supports the conclusion that the model detects a physically real structure–conductivity relationship rather than fitting noise. However, with n = 23, no strong statistical claims can be made. Additional in-house data collection is in progress.

*ML Framework Validation Summary*

Figure 22 below summarizes the complete three-step validation framework developed for this Work Area. It shows how the three datasets (HTP-MD simulation data, Bradford experimental literature, and in-house EIS measurements) map onto the three distinct validation questions, what feature vectors were used at each step, and the resulting MAPE outcomes. This diagram captures the current state of validation and serves as the reference point for tracking future progress as additional data and properties are incorporated.

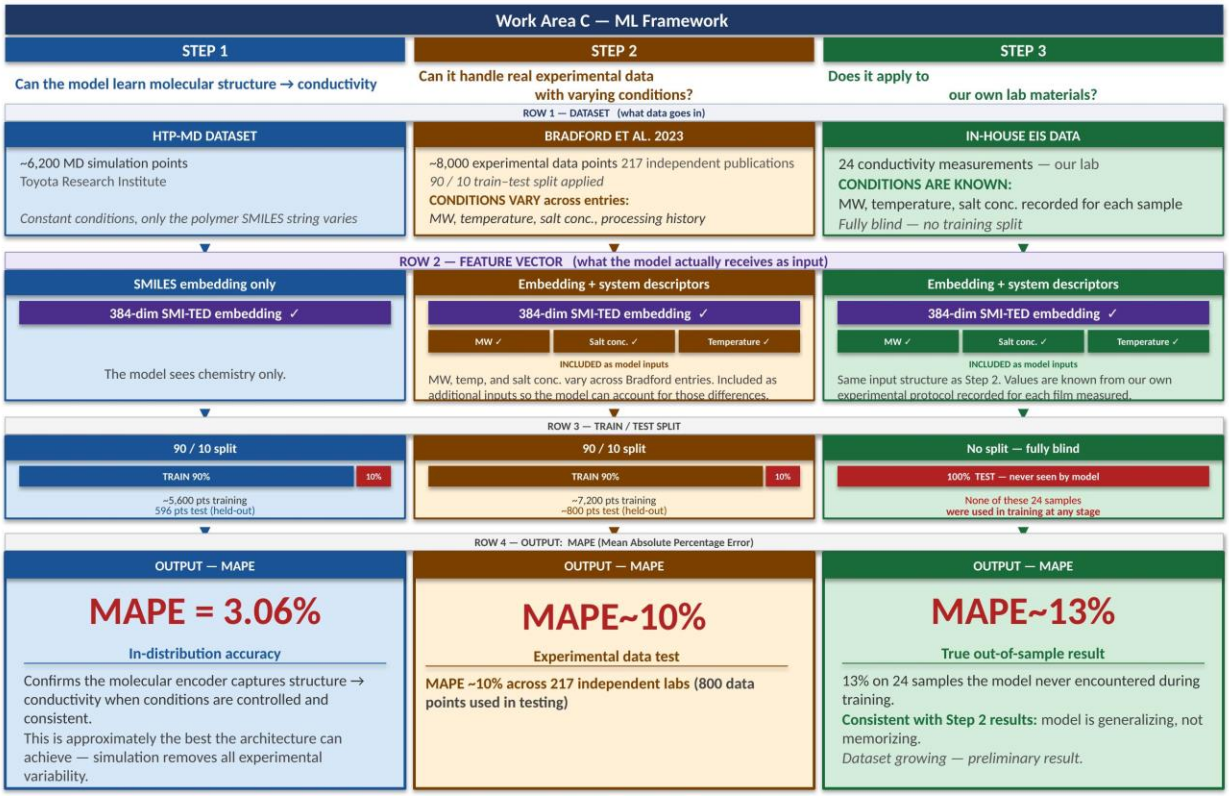


*Figure 22. Work Area C — ML Framework Validation Summary. The three-column layout shows the three sequential validation steps: (Step 1) in-distribution accuracy on simulation data (MAPE = 3.06%); (Step 2) cross-distribution transfer to experimental literature data (MAPE ≈ 10%); (Step 3) out-of-sample prediction on in-house lab materials (MAPE ≈ 13%). Color coding distinguishes dataset type, feature vector composition, and train/test split at each step.*

## E. PROJECT RESULTS

**Please provide a narrative describing the key results using the project's milestones as sub-headings.**

- Describe the importance of the key results.
- Include a discussion of the project specific metrics and variances between expected and actual performance.

**Work Area A**

On the microgrid scale a degradation aware energy management system was designed and tested in a realistic simulation. The EMS reduced annual operating costs by up to $500K for a 10 MWh system compared to alternative approaches, providing cost savings of approximately 2.7% while maintaining linearity and computational efficiency.

***Operational Cost Reduction and Battery Lifespan***

Three distinct degradation modeling methods were proposed for implementation and comparison to accurately represent and incorporate battery energy storage systems (BESS) degradation. Of the three models, the LNN provided the best solution, achieving lower operating costs with depreciation compared to alternative approaches. Costs remain nearly identical across all degradation modeling methods for battery sizes up to 6 MWh, however, for 8- and 10-MWh systems, the LNN approach yields noticeably lower costs, reducing overall campus operating expenses by 2.6%.

The hybrid approach to modelling the campus microgrid it was possible to modify the size of the battery and its C-rate. In all cases, the LNN model provided the best energy management. It extended the lifetime of the battery as compared to the other two EMS and led to reduced annual operating costs by up to $500K for a 10 MWh system compared to alternative approaches.

**Work Area B**

A modular modelling framework was developed to model power systems. The advantage of this modelling approach is that components can be added and removed without changing the dynamics of other components in the model. In addition, with proper measurements, the dynamics of the components can be estimated from data (again without bias due to other components in the grid). This approach was successfully applied to estimate and monitor the dynamics of a battery connected to a small grid.

***Transfer Function***

The work completed in this Work Area allowed for linking between a transfer function of a battery and the physics of the battery. The transfer function of the battery was estimated from data, and from this transfer function was possible to infer physical characteristics of the battery and demonstrated with strong model fitness (RMSE of 0.014 $\pm$0.0034 V).

***Particle Model with Electrolyte (SPMe) Model***

The SPMe model of a battery was used to infer that the pole locations of the transfer function of a battery are proportional to the electrolyte diffusivity coefficient. Based on results from this Work Area a typical SPMe representation was transformed into a state-space representation using spatial discretization. The main insights that are obtained from this derivation include:

- A lithium-ion battery can be represented as a linear dynamic block followed by nonlinearity. The state update equation was linear (in $x$ and $I$)., whereas the output equation is nonlinear (in $x$ and $I$).
- The dynamics are only a function of the diffusion coefficient of the electrolyte. This is a key observation since the poles of an estimated transfer function are only a function of the diffusion coefficient of the electrolyte.

***Modular Model Approach***

A modular model of a power system was developed using a port-Hamiltonian model, which allowed components to be added or removed from the model. The current model developed and tested includes a battery, inverter, and load and simulated testing results were within the 95% confidence interval using the utility scaled microgrid performance data and a simulated lithium-ion battery. The predictive model had a low prediction error of about 4% overall. The model also demonstrated that Battery dynamics can be estimated from battery terminal voltage and current readings, and changes to charge transfer resistance can be tracked.

It is anticipated that the developed physics-based algorithm can be applied to more complex microgrids (with multiple batteries, solar panels, etc.), which will further showcase the advantages of the modular modelling approach used for this project.

**Work Area C**

On the materials side, this project demonstrates the successful application of a molecular foundation model to the prediction of transport properties in solid polymer electrolytes. To our knowledge, this work represents the first use of the SMI-TED foundation model for polymer electrolyte materials, extending large-scale chemical representation learning into this domain. The results show that pretrained molecular embeddings, combined with experimentally relevant descriptors, can capture key chemistry–transport relationships governing ionic conductivity.

***Multi-Scale Data Integration***

The Work Area C framework operates at the material scale, but it is designed as one component within a three-scale pipeline that spans from molecular chemistry to microgrid operation. Understanding how data flows between the three scales — and where the connections currently stand — is essential context for interpreting the validation result findings.

***Scale 1: Material Scale***

At the material scale, the primary model prediction is ionic conductivity, from molecular structure (SMILES) and system descriptors (molecular weight, salt concentration, temperature). The three-step validation described in this report operates entirely at this scale. The outputs — predicted conductivity as a function of polymer chemistry and formulation conditions — are the quantity of interest for material selection and inverse design.

The material scale framework is agnostic to how the electrolyte will be used in a device. Its role is to screen and rank candidate materials based on transport properties alone, providing a shortlist of promising formulations that can be passed to device-level evaluation.

***Scale 2: Battery/Device Scale***

At the battery scale, Work Area C used cycling data and accelerated aging data to parameterize and validate electrochemical cell models. The key inputs at this scale are capacity retention as a function of cycle number, rate capability curves (discharge capacity vs. C-rate), impedance evolution over cycle life, and Coulombic efficiency. These quantities are obtained from coin cell and full-cell experiments using the same SPE formulations characterized at the material scale.

The material scale and battery scale are connected through the ionic conductivity of the electrolyte: the ML framework predicts conductivity for a given formulation, and that predicted conductivity is used as an input parameter in the equivalent circuit and electrochemical models used by the device team. As more in-house coin cell cycling data is generated, this connection will become increasingly direct — moving from using bulk conductivity as a proxy to directly validating device performance predictions against cycling observations.

***Current State of Integration***

As of the end of this project, the three scales are operating as semi-independent validation domains. The material scale has demonstrated preliminary predictive capability for ionic conductivity. The battery scale team is using in-house cycling data to validate device models. The microgrid scale uses simulated battery models.

What has not yet been achieved is a fully integrated, end-to-end pipeline where a predicted material property flows automatically through the battery model into the microgrid simulation. Establishing that end-to-end connection is identified as a priority for the next milestone, with Integration between scales is progressing. The full end-to-end pipeline is targeted for the future work, which includes:

- incorporating the conductivity information from the ML framework into material design;
- gathering data on cycling, accelerated aging, and overall performance at coin cell scale; and
- simulating load and dispatch using the battery model outputs at a microgrid scale.

***Limitations***

Importantly, these results also highlight current limitations: processing history, crystallinity, and morphology are not represented in 1D structural encodings; mechanical properties and dendrite suppression remain outside the current prediction scope; and the in-house dataset is not yet large enough to support definitive statistical conclusions.

These are recognized gaps with clear improvement pathways, not fundamental architectural constraints.

## F. KEY LEARNINGS

**Please provide a narrative that discusses the key learnings from the project.**

- Describe the project learnings and importance of those learnings within the project scope. Use milestones as headings, if appropriate.
- Discuss the broader impacts of the learnings to the industry and beyond; this may include changes to regulations, policies, and approval and permitting processes

*RESPOND BELOW*

**Work Area A – Microgrid Energy Management System**

The key learning in this work area was that the LNN method provided the best solution. Because of the hybrid approach to modelling the campus microgrid it was possible to modify the size of the battery and its C-rate. In all cases, the LNN model provided the best energy management. It extended the lifetime of the battery as compared to the other two EMS and led to reduced annual operating costs by up to $500K for a 10 MWh system compared to alternative approaches. This is a very interesting result and will guide future work on degradation aware EMS. Specifically, to incorporate more types of ML methods into battery management systems.

It is also important to implement the EMS on a physical microgrid for a more complete validation of the method. This will be done on the University of Calgary research microgrid.

**Work Area B – Data Driven Modelling**

***Modular Data Driven Modelling***

One of the key learnings in this work area was that the port-Hamiltonian based battery model was able to fit real data very well. The data set investigated in this project consisted of one battery connected via inverters to the grid. It will be interesting to apply this algorithm to more complex microgrids (with multiple batteries, solar panels, etc.). This will showcase the advantages of our modular modelling approach even more.

***Validation***

It was difficult to validate the approach fully. Although it was possible to validate that the model is capturing all the information in the data, more work is required to validate the physical interpretation of the estimated dynamics.

For example, one of the real data sets used was from a vanadium redox flow battery connected to power electronics and a load. However, due to time constraints, a physics-based model for vanadium redox flow batteries were not available. This is important work and it will continue in the coming months.

Even with a physics-based model, it was difficult to validate the estimated models. For the lithium-ion cycle testing data, it was possible to monitor the battery degradation. However, even with the physics based SPMe model, it is difficult to fully validate the estimated model because it is difficult to know exactly how the battery is degrading during the cycle testing. Further validation work is required in this case, possibly with specialized cycle testing where extra parameters are measured during the cycle testing, or periodically during the cycle testing.

**Work Area C – Materials Selection**

***Literature Data Availability and Quality***

The most significant practical challenge encountered in this work was the limited availability of high-quality, standardized training data for solid polymer electrolytes. While the Bradford et al. (2023) dataset represents the most comprehensive currently available compilation, it remains a collection of heterogeneous measurements from 217 independent publications with differing synthesis routes, measurement protocols, reporting conventions, and levels of completeness. A significant number of entries were missing one or more descriptor values (e.g., molecular weight was not reported alongside conductivity), requiring manual curation that itself introduced judgment calls about data inclusion.

The incompleteness of the raw Bradford dataset before curation, and the meaningful improvement in MAPE (from 20.7% to 10.3%) after manual removal of NaN entries, underscores how sensitive model performance is to data quality. Building curated, standardized datasets for SPE properties remains an open challenge for the field, not just for this project.

***Historical Data Bias: Conductivity Underestimation***

An important finding with direct practical implications is that the model systematically underestimates conductivity for the in-house samples. Investigation of the Bradford training data revealed that a substantial fraction of the literature entries date from earlier periods when sample preparation techniques, glovebox protocols, and EIS measurement procedures were less refined than those used today. As a result, conductivity values reported for the same polymer–salt system in older publications are consistently lower than values measured with modern techniques.

Because the model was trained predominantly on this historical distribution, it inherits this systematic downward bias. Researchers have, over time, substantially improved how these experiments are conducted — better moisture control, more rigorous drying protocols, improved equivalent circuit fitting — and these improvements are reflected in more recent measurements but not yet in the training dataset. Correcting for this temporal bias will require either weighting more recent publications more heavily or incorporating a specific correction factor for data vintage. This is identified as a concrete improvement target.

***Mechanical Property Data Scarcity***

Young's modulus and other mechanical strength parameters (tensile strength, elongation at break, creep resistance) are particularly scarce in the SPE literature. In contrast to conductivity, which has been measured for thousands of formulations, mechanical data are available for only a small fraction of characterized polymer electrolytes. This severely limits the ability to train a predictive model for mechanical properties using the current approach.

This is a known gap in the field and is one of the reasons that the present framework focused on conductivity as the entry point. Extending the framework to mechanical properties will require a targeted data collection campaign, likely through a combination of in-house measurements and community-level data-sharing efforts — before machine learning approaches can be meaningfully applied.

***Small In-House Dataset Size***

The in-house experimental dataset currently contains only about 23 data points, each representing a different temperature measurement of a small number of film batches. EIS characterization is experimentally demanding: preparing a batch, ensuring complete drying, storing under inert atmosphere, and measuring across multiple temperatures requires several weeks per batch. As a result, growing the in-house dataset to a size that would support robust statistical conclusions is a medium-term effort, not something achievable within a single milestone. The current result is presented as a preliminary indicator, not a statistically definitive validation.

***Model Scope: What the Framework Cannot Predict and Limitations***

The current framework predicts bulk ionic conductivity from chemical structure and system descriptors. It does not predict:

1. Interfacial resistance between the electrolyte and the electrode, which is a major determinant of cell performance at high rates.
2. Mechanical modulus or tensile properties, due to data scarcity.
3. Dendrite suppression capability, which depends on modulus, interfacial stability, and morphology not captured in 1D structural encodings (this was discussed in Milestone 2 as a key challenge, and the limitation persists).
4. Electrochemical stability window, though this is a planned future extension once suitable datasets are identified.
5. Degradation or aging behavior under cycling conditions.

Each of these limitations represents a pathway for future model extension as appropriate datasets become available.

**Overall Project Learnings**

***Ambitious Scope***

The original project proposal was very ambitious. This became quite clear in the final milestone. Multiple aspects of the project were ambitious in terms of effort, time, and costs.

Several project activities required more time than initially anticipated, particularly the validation of both the data-driven model and the AI-based predictive model. Additionally, developing a battery degradation model within the project timeline proved unrealistic.

The primary reason for the delay in validating the data-driven model for the flow battery was that, by the end of Milestone 1, only a physics-based model for lithium-ion batteries—one that could be identified from data—had been developed. There was insufficient time to create an equivalent model for flow batteries, and this step ultimately required significantly more effort than expected. The extended timeline was driven partly by the steep learning curve associated with understanding lithium-ion battery behavior, and partly by the sheer number of physics-based models available in the literature. After extensive review, a model was selected that offered an appropriate balance between physical accuracy and a structure in which parameters could be uniquely estimated from data.

The AI component of the project also progressed more slowly than planned. A substantial learning curve was involved in selecting a suitable neural network architecture, as many candidate structures exist in the

literature and determining the most appropriate option required considerable research. Furthermore, collecting, organizing, and preprocessing the required data for training introduced additional delays. Despite these challenges, the project successfully produced a promising predictive AI model. However, due to the extended time required to reach this stage, the development of the originally proposed generative AI model was not completed.

In future project proposals these learnings will be considered to propose timelines and scopes of work that are more realistic.

## G. OUTCOMES AND IMPACTS

**Please provide a narrative outlining the project's outcomes. Please use sub-headings as appropriate.**

- **Project Outcomes and Impacts:** Describe how the outcomes of the project have impacted the technology or knowledge gap identified.
- **Clean Energy Metrics:** Describe how the project outcomes impact the Clean Energy Metrics as described in the *Work Plan, Budget and Metrics* workbook. Discuss any changes or updates to these metrics and the driving forces behind the change. Include any mitigation strategies that might be needed if the changes result in negative impacts.
- **Program Specific Metrics:** Describe how the project outcomes impact the Program Metrics as described in the *Work Plan, Budget and Metrics* workbook. Discuss any changes or updates to these metrics and the driving forces behind the change. Include any mitigation strategies that might be needed if the changes result in negative impacts.
- **Project Outputs:** List of all obtained patents, published books, journal articles, conference presentations, student theses, etc., based on work conducted during the project. As appropriate, include attachments.

*RESPOND BELOW*

**Project Outcomes and Impacts**

The project initially identified a key gap between materials science and power engineering:

- **Materials scientists** require insight into how batteries degrade under real microgrid operating conditions to design chemistries and structures that achieve longer lifetimes.
- **Power engineers** need accurate knowledge of battery degradation mechanisms so that this information can be embedded into energy management systems, enabling more efficient and cost-effective battery operation.

The work completed in this project has made significant progress toward addressing these gaps across three main work areas.

**Project Specific Metrics**

***TRL Advancement***

When the project started, the technology readiness level (TRL) of the technology in all three work areas were at a proof-of-concept level of development aligning with an Alberta Innovates' definition of TRL 3. The work completed during this project with regards to degradation aware energy management systems

(Work Area A), data driven monitoring (Work Area B), and AI driven material selection (Work Area C) were all advanced in TRL.

In Work Area A (Algorithms for Energy Management Systems) the degradation aware EMS was tested on hybrid real and simulated data. Several technological components were integrated into the framework including degradation models, energy managements systems, and all the components in the microgrid. The framework was tested in a realistic simulation study. This aligns with the conditions for TRL 5 where "at this level the basic technological components are integrated for testing in a simulated environment." The immediate next step involves simulating in an operational environment, which aligns with TRL 6.

In Work Area B (Data Driven Modelling) the final algorithm was tested on real data to monitor changes in the physical parameters of batteries. Again, several components were integrated into the framework including physics-based models of batteries, data driven modelling algorithms, and the port-Hamiltonian modelling framework. The resulting integrated framework was tested on real data. The model was only partially validated from a physics point of view. Therefore, the TRL aligns somewhere between 4 and 5.

In Work Area C (Material Selection) the final ML model was partially validated on both simulated and experimental data. The model integrated several components including SMILES and LLMs. The model was trained to estimate ionic conductivity of polymers. Because the ML algorithm was only partially validated, the TRL is somewhere between 4 and 5.

***Students Trained***

Students trained during this project are shown in the following table.

| *Work Area* | *Number of HQP trained* |
|---|---|
| *Microgrid team* | 1PDF, 1Ph.D., 1M.Sc. |
| *Data driven monitoring team* | 1Ph.D., 1 M.Sc. |
| *AI driven material selection team* | 1PDF, 1M.Sc. |

In total, 2 PostDocs, 2 Phd, and 3 MSc students were trained. Both Ph.D. students will continue their studies by working on extensions of the work completed in this project. The M.Sc. from the microgrid team is preparing to graduate and is looking for jobs in the power systems industry. The M.Sc. from the data driven monitoring team is also preparing to graduate and looking for jobs in the battery industry. The M.Sc. from the materials group has continued working in energy storage technology is doing a Ph.D. in the same group.

***Publications***

Currently three conference publications have been accepted:

- European Research Network on System Identification (ERNSI) Workshop 2025 in Bordeux, France where a poster was presented titled "Robust Nonlinear Modeling of Grid-Connected Power Systems Using a Port-Hamiltonian Approach", by Mahsan Ghasemi and Arne Dankers.

- IEEE Electrical Power and Energy Conference 2025 in Waterloo, Canada. Presenation titled “Stochastic Planning of a Campus Microgrid Considering Practical CHP and Market Constraints” by. Masoud Foroushani and Mostafa Faroukhabadi.
- Electrochemical Society Meetings in Montreal, Canada. Presentation titled “Functionally Optimized Low Loading Electrodes for PEM Water Electrolyzers” by Monissh Vijayakumar and Mayank Sabharwal.

Two conference papers and two journal papers are currently being prepared. Two are in the advanced stages of writing and one conference paper and one journal paper are still in the planning stages.

***Knowledge Mobilization***

One conference publication has been published and three more are under development. There are plans to submit a journal paper in the coming months.

One journal paper will cover the work from the microgrid team and be submitted to IEEE Transactions on Smart Grids.

Another journal paper covering the work of the materials group on predictive AI is in the planning stages.

One conference paper on battery monitoring using the port-Hamiltonian modelling framework has been submitted to IEEE Energy Conversion Conference and Expo 2026.

Another conference paper on estimating physical properties of a battery from data is being prepared.

***Existing Sector HQP Retained***

All 10 professors remain at the university and continue to conduct research in batteries.

***Number of Technologies/Features Developed in Association with the Project***

The project target was to have three technologies developed in association with the project, one for each work area accordingly:

***Work Area A*** **- Degradation-informed scheduling strategies of energy storage devices within a microgrid**

The microgrid team has designed and implemented a degradation-aware energy management systems that can incorporate the output of the monitoring algorithm. The result is a reduction in operating costs of a microgrid.

***Work Area B*** **- Data-driven physics-based algorithm development for energy storage devices**

A monitoring algorithm has been developed and implemented capable of estimating and monitoring changes in the battery dynamics from operational data.

The results of the monitoring algorithm can now inform the materials team regarding identifying degradation roots causes associated with batteries in operation. It can also the microgrid team regarding models regarding future research in battery degradation.

***Work Area C - Material selection based on energy storage device physics***

A model was developed to predict battery properties given the chemistry and structure. This work forms foundational efforts towards a generative AI capable of recommending new battery chemistries and structures that will result in prolonged battery life as it relates to degradation issues.

## H. BENEFITS

**Please provide a narrative outline the project's benefits. Please use the subheadings of Economic, Environmental, Social and Building Innovation Capacity.**

- **Economic:** Describe the project's economic benefits such as job creation, sales, improved efficiencies, development of new commercial opportunities or economic sectors, attraction of new investment, and increased exports.
- **Environmental:** Describe the project's contribution to reducing GHG emissions (direct or indirect) and improving environmental systems (atmospheric, terrestrial, aquatic, biotic, etc.) compared to the industry benchmark. Discuss benefits, impacts and/or trade-offs.
- **Social:** Describe the project's social benefits such as augmentation of recreational value, safeguarded investments, strengthened stakeholder involvement, and entrepreneurship opportunities of value for the province.
- **Building Innovation Capacity:** Describe the project's contribution to the training of highly qualified and skilled personnel (HQSP) in Alberta, their retention, and the attraction of HQSP from outside the province. Discuss the research infrastructure used or developed to complete the project.

*RESPOND BELOW*

**Economic Benefits**

The commercialization of this project could significantly impact the energy sector by reducing operational and maintenance costs for microgrids, enhancing the reliability and efficiency of energy storage systems, and potentially lowering energy prices for consumers. By improving the integration and management of renewable energy sources, it could also accelerate the transition to sustainable energy, driving economic growth in green technologies. Additionally, the development of scalable and modular microgrid solutions could open new markets and create jobs in manufacturing, installation, and maintenance, contributing to economic development and energy independence.

The National Renewable Energy Laboratory estimates that microgrids cost $2 million-$4 million per MW, and that's without accounting for location, energy mix and purpose. Therefore, just on the installation of the modular microgrids, enabled by the enhanced energy management, the savings taken as 20% of the total cost are $400-800k per MW. Increased adoption of microgrid systems would lead to savings on capital and maintenance and capital expenditure for construction of electricity transmission systems up to isolated, rural communities. For instance, the estimated cost of conventional overhead transmission lines is about $1.5 - $ 2 million per kilometer (www.gridnorthpartners.com, 2021). On the other hand, the total estimated cost to set up a microgrid is around $2 - 4 million/MW, (www.microgridknowledge.com,

2020) making them a much more affordable option for communities. Furthermore, natural calamities such as tornadoes, forest fires and lightning strikes may cause substantial damage to power transmission lines. Microgrids may lead to substantial savings in such situations, owing to their distributed nature

**Environmental Benefits**

The key environmental impact of this project is to enable more efficient operation of batteries in microgrids. This includes prolonging the life of a battery by including degradation aware energy management systems. By promoting microgrids, the integration of renewable energy sources also becomes more feasible. This has clear environmental benefits.

The National Renewable Energy Laboratory (NREL) has undertaken extensive reviews and harmonizations of life cycle assessments (LCAs) for electricity generation technologies, including renewable energy systems and storage technologies (https://www.nrel.gov/docs/fy13osti/57131.pdf ). This effort aims to reduce variability in LCA results, making them more comparable and useful for decision-making. The harmonization process has shown that renewable energy technologies, such as solar and wind, generally have almost 10x lower and less variable life cycle greenhouse gas (GHG) emissions compared to combustion-based natural gas and coal technologies. Therefore, wider microgrid adoption would significantly lower the associated GHG emissions.

LCA studies typically show that while energy storage components have upfront emissions from manufacturing and material extraction, their lifetime emissions are significantly lower compared to fossil fuel-based systems. These emissions vary from one to another and storage technology and is highly dependent on the technology readiness. In all cases, extending the lifetime of an energy storage device (as was done in this project) will reduce the lifetime emissions of the device.

## I. RECOMMENDATIONS AND NEXT STEPS

**Please provide a narrative outlining the next steps and recommendations for further development of the technology developed or knowledge generated from this project. If appropriate, include a description of potential follow-up projects. Please consider the following in the narrative:**

- Describe the long-term plan for commercialization of the technology developed or implementation of the knowledge generated.
- Based on the project learnings, describe the related actions to be undertaken over the next two years to continue advancing the innovation.
- Describe the potential partnerships being developed to advance the development and learnings from this project.

*RESPOND BELOW*

**Work Area A**

The work completed in this project will be continued by developing a forecast-free degradation-aware operating policy for solar-coupled lithium-ion BESS that maximizes discounted lifetime value while enforcing explicit battery health guarantees. The novelty is to replace the typical reliance on energy

forecasting systems, e.g., PV and price predictors with a principled 'online learning' control that reacts to observations and uncertainty in real time. Methodologically, the controller consists of a two-layer structure:

1. A real-time predictor-free online optimizer that updates BESS setpoints from the most recent measurements using a convex-learning update with inertia/momentum to avoid harmful charge and discharge chattering.
2. A degradation-and-safety shield that certifies each action against battery aging and operational limits. The shield will be trained from data using an embedded degradation surrogate that can be co-optimized inside the learning policy, rather than approximating it externally.

Outcomes will include:

- A set of interpretable operating strategies, e.g., shallow-vs-deep cycling regimes and seasonal/temperature-aware aggressiveness schedules with explicit cycle-life/value trade-offs.
- A benchmarked policy suite against Mixed Integer Linear Programming (MILP) baselines under photovoltaic (PV) and price uncertainty.
- A deployment-ready controller that delivers higher discounted lifetime profit while meeting end-of-life and annual fade/cycle constraints through degradation-aware co-optimization.

**Work Area B**

The implementation of the port-Hamiltonian modelling framework to power systems will continue to be used and developed. The battery monitoring algorithms will be expanded to include temperature effects for monitoring of batteries in cold climates and potentially also in conjunction with data centers as loads, to investigate the effect of this type of load on battery degradation.

A second extension of the modular model of the power system involves monitoring the inverters instead of the batteries. These can also be monitored using essentially the same algorithm developed in this project. This could be important for system operators, as is described below.

The power grid is currently experiencing a rapid change and will soon be dominated by power electronic converters, primarily driven by the increased percentage of renewable energy generation, electric vehicle charging capacity and data centers being installed and connected.

A power electronic converter dominated grid presents unique challenges as power converters are non-linear elements. There are two issues:

1. Grid frequency oscillations grid associated with inductive and capacitive loads.
2. Nonlinear elements can amplify these oscillations resulting in voltage distortion which can lead to equipment malfunctioning like nuisance tripping, exciting resonant frequencies, line overloading and electro-magnetic interference.

To mitigate these negative effects, electric system operators require knowledge of components in the grid causing the nonlinear distortions. Using the port-Hamiltonian based model of a power system developed in this project, the inverters can also be monitored (instead of the batteries). Specifically, the inverters can be monitored for severe nonlinear behaviour which enables system operators to locate devices in the grid that are a potential source of distortion.

**Work Area C**

The immediate next step is to expand the in-house experimental dataset to a size that supports more robust statistical conclusions. This includes additional PEO-based formulations with varied salt concentrations and molecular weights, and selected novel polymer chemistries for which the model's transferability can be tested. Simultaneously, the training dataset will be updated to incorporate more recent literature data, reducing the historical conductivity bias identified in this milestone.

Transference number prediction will be added as a second property target, using the same molecular embeddings but a separate prediction head. This will directly test the architectural generality claim and provide a practically important prediction for electrolyte design.

**All Work Areas - Connecting the Scales**

***Integrate Material Scale and Battery Scale***

The material scale framework (ionic conductivity predictions) and the device scale framework (electrochemical cell models, cycling data) need to be formally connected. The planned integration pathway includes predicted conductivity values from the ML model will be fed directly into the equivalent circuit parameterization used by the device team. In parallel, coin cell cycling data from in-house experiments will be used to validate the device model predictions, creating a closed loop where material properties predict device behavior, and device behavior validates material predictions. This integration is the most consequential near-term development target for Work Area C.

The two scales currently operate on the same materials but have not yet been formally linked in a single computational pipeline. Establishing this link will enable the framework to answer device-relevant questions (e.g., "which formulation maximizes cycle life at a given power requirement?") rather than material-relevant questions alone (e.g., "which formulation maximizes conductivity?").

***End-to-End Connection to Microgrid***

Once the material–battery scale link is established, the next step is to propagate material and device-level predictions upward to the microgrid simulation. The goal is an end-to-end pipeline in which a candidate polymer formulation can be evaluated not only for its conductivity, but for its expected contribution to system-level metrics such as energy efficiency, cycling lifetime, and round-trip efficiency under realistic grid demand profiles.

This end-to-end connection will require:

1. Automated handoff of battery model parameters from validated device simulations to the microgrid simulator.
2. Uncertainty quantification at each scale so that prediction confidence propagates through the pipeline.
3. A feedback mechanism that allows microgrid-level performance targets to inform material-scale search criteria (i.e., inverse design from grid requirements downward to chemistry).

This last capability is the long-term vision of the framework and represents the core innovation of the integrated multi-scale approach.

## J. KNOWLEDGE DISSEMINATION

**Please provide a narrative outlining how the knowledge gained from the project was or will be disseminated and the impact it may have on the industry.**

*RESPOND BELOW*

**Conferences:**

Currently one conference publication has been published, two conference presentations/posters were presented with a published abstract only, one conference paper has been submitted (acceptance not know at time of writing this report).

Two conference papers and two journal papers are currently being prepared. Two are in the advanced stages of writing and one conference paper and one journal paper are still in the planning stages.

***Conference presentations/posters with only a published abstract:***

Mahsan Ghasemi and Arne Dankers. "Robust Nonlinear Modeling of Grid-Connected Power Systems Using a Port-Hamiltonian Approach" European Research Network on System Identification (ERNSI) Workshop 2025 in Bordeux, France.

Monissh Vijayakumar and Mayank Sabharwal. "Functionally Optimized Low Loading Electrodes for PEM Water Electrolyzers". Electrochemical Society Meetings in Montreal, Canada.

***Published conference paper:***

MH Foroushani, M Farrokhabadi. Stochastic Planning of a Campus Microgrid Considering Practical CHP and Market Constraints. 2025 IEEE Electrical Power and Energy Conference (EPEC), pp170-176, 2025.

***Submitted conference paper:***

A. Ghasemi, A. Dankers. Nonlinear Port-Hamiltonian Modeling for Parameter Identification and Degradation Analysis of Grid-Connected Battery. Submitted to IEEE Energy Conversion Conference and Expo 2026.

**Papers**

***Papers in Preparation:***

One journal paper currently in preparation will cover the work from the microgrid team and be submitted to IEEE Transactions on Smart Grids. The current working title of the paper is "Benchmarking Battery Energy Storage Degradation Methods in Microgrids Energy Management Systems".

A journal paper covering the work of the materials group on predictive AI is in the planning stages.

A conference paper on estimating physical properties of a battery from data is being prepared.

## K. CONCLUSIONS

**Please provide a narrative outlining the project conclusions.**

- Ensure this summarizes the project objective, key components, results, learnings, outcomes, benefits and next steps.

*RESPOND BELOW*

**Project Objectives**

The technology development project focused on a multi-disciplinary approach aimed at integrating material science, data driven models, and power systems engineering to develop a platform to monitor battery degradation during operation in microgrids.

Advancements towards this objective were achieved and work to achieve the desire platform is ongoing.

**Key Components and Results**

**Work Area A**

On the microgrid scale a degradation aware energy management system was designed and tested in a realistic simulation. The EMS reduced annual operating costs by up to $500K for a 10 MWh system compared to alternative approaches, providing cost savings of approximately 2.7% while maintaining linearity and computational efficiency.

**Work Area B**

On the data driven modelling side, a modular modelling framework was developed to model power systems. The advantage of this modelling approach is that components can be added and removed without changing the dynamics of other components in the model. In addition, with proper measurements, the dynamics of the components can be estimated from data (again without bias due to other components in the grid). This approach was successfully applied to estimate and monitor the dynamics of a battery connected to a small grid.

**Work Area C**

The project work completed for this Work Area demonstrates the successful application of a molecular foundation model to the prediction of transport properties in solid polymer electrolytes. To our knowledge, this work represents the first use of the SMI-TED foundation model for polymer electrolyte materials, extending large-scale chemical representation learning into this domain.

The results show that pretrained molecular embeddings, combined with experimentally relevant descriptors, can capture key chemistry–transport relationships governing ionic conductivity. The model achieves high predictive accuracy on the internally consistent HTP-MD simulation dataset (MAPE = 3.06%), competitive performance on heterogeneous experimental literature data (MAPE ≈ 10.3% after curation), and a preliminary out-of-sample result on in-house measurements (MAPE ≈ 13% on n = 23).

The results provide evidence of a physically including a structure conductivity relationship, which has been partially quantitatively validated, and is limited by in-house dataset size, historical bias in the training data, and absence of independent multi-lab replication. Ongoing experimental work is directly targeted at addressing these gaps.

Importantly, the results also highlight current limitations: processing history, crystallinity, and morphology are not represented in 1D structural encodings; mechanical properties and dendrite suppression remain outside the current prediction scope; and the in-house dataset is not yet large enough to support definitive statistical conclusions. These are recognized gaps with clear improvement pathways, not fundamental architectural constraints.

The framework established in this work provides a scalable foundation for data-driven electrolyte discovery and multi-scale integration. Because the molecular encoder is property-agnostic, the same latent chemical representation can be reused to train predictive models for additional electrolyte properties. The three-scale pipeline connecting material properties, device performance, and microgrid operation is the ultimate target, and the current work represents a validated first step toward that objective.

**Learnings and Outcomes**

One learning was that the proposed project was very ambitious.

Two components of the original project could not be fully addressed during this project timeline:

1. Development of a degradation model based on the monitoring algorithm developed in this project.
2. A generative AI based on the predictive AI developed in this project. In addition, some of the results require further validation and testing.

For the microgrid scale, the key learning is that it appears that ML based EMSs out performs more standard implementations of EMS, which will be further explored in future work.

The key learning on the data driven modelling work identified that dynamic models best fit battery dynamics when individual components are well estimated and appropriate network modelling tools are used. Further work is required to validate the interpretation of the estimated dynamics in terms of degradation of the battery.

The work completed for the materials group developed a model with very high accuracy. However, the results also highlight several limitations including:

1. Processing history, crystallinity, and morphology are not represented in 1D structural encodings.
2. Mechanical properties and dendrite suppression remain outside the current prediction scope; and
3. The in-house experimental dataset is not yet statistically large enough to support definitive validation conclusions.

These are recognized gaps with clear improvement pathways, not fundamental architectural constraints.

**Benefits and Next Steps**

The framework established in this work provides a scalable foundation for data-driven electrolyte discovery and multi-scale integration. The three-scale pipeline connecting material properties, device performance, and microgrid operation is the ultimate target, and the current work represents a validated first step toward that objective.

The key benefits of this framework will ultimately lead to drastically reduced design cycles for material selection of batteries, batteries that are designed to withstand degradation in real operating conditions,

and energy management systems that balance degradation and power needs. Each of these benefits result in lower costs for building and operating microgrids.

Work continues each the of the three sub-projects. In the immediate future, the focus is on further validation, and on more integration between the work areas. In the longer term we envision adding more components to the framework. For instance, it can be applied to electrolyzers and other types of batteries.

Once deployed on a live microgrid, this platform will reduce the development time of battery design, lead to a better understanding of battery degradation, reduce the cost of operating a microgrid and resulting in a more sustainable microgrid.

**References**

Alberta Electric System Operator (AESO). Accessed: Sep. 15, 2024. [Online]. Available: https://www.aeso.ca/, 2023

Bradford, G., Lopez, J., Ruza, J., Stolberg, M. A., Osterude, R., Johnson, J. A., . . . Shao-Horn, Y. (2023). Chemistry-Informed Machine Learning for Polymer Electrolyte Discovery. *ACS Central Science.*

Brosa Planella, F. et al. (2022). A continuum of physics-based lithium-ion battery models reviewed. *Progress in Energy*, vol. 4, 042003.

Derr, I.; Przyrembel , D.; Schweer, J.; Fetyan, A.; Langner , J.; Melke , J.; Weinelt, M.; and Roth, C. (2017) Electroless chemical aging of carbon felt electrodes for the all-vanadium redox flow battery (VRFB) investigated by Electrochemical Impedance and X-ray Photoelectron Spectroscopy. *Electrochimica Acta*, Volume 246, pp 783-793.

Foroushani, M.H. and Farrokhabadi, M. (2025). Stochastic planning of a campus microgrid considering practical CHP and market constraints. *2025 IEEE Electrical Power and Energy Conference (EPEC)*, pp. 170‑176.

Grimaldi, A., Minuto, F.D., Perol, A., Casagrande, S., and Lanzini, A., (2025). Techno-economic optimization of utility-scale battery storage integration with a wind farm for wholesale energy arbitrage considering wind curtailment and battery degradation. *Journal of Energy Storage*, vol. 112, p. 115500.

HTP-MD (High-Throughput Polymer Design - Molecular Dynamics). (2023). Retrieved from https://www.htpmd.matr.io/

Ljung, L. (1999). System identification: theory for the user (second edition); Prentice-Hall, Englewood Cliffs, NJ, 1999.

Marti-Florences, M., Cecilia, A.,, and Costa-Castello, R. (2023). Modelling and Estimation in Lithium-Ion Batteries: A Literature Review. *Energies*, vol. 16, 6846.

Moura, S.J., Bribiesca Argomedo, F., Klein, R., Mirtabatabaei, A., and Krstic, M. (2017). Battery State Estimation for a Single Particle Model With Electrolyte Dynamics. *IEEE Transactions on Control Systems Technology*, vol. 25, no. 2, pp. 453‑468

National Renewable Energy Laboratory (2024). 2024 annual technology baseline: Commercial battery storage. Accessed: Feb. 15, 2025. [Online]. Available: https://atb.nrel.gov/electricity/2024/commercial battery storage, 2024.

Xie, T., et al. (2023). High-throughput polymer electrolyte design using molecular dynamics simulations. APL Machine Learning.

Yesilyurt, M.S.; Yavasoglu, H.A. (2023) An All-Vanadium Redox Flow Battery: A Comprehensive Equivalent Circuit Model. *Energies*, *16*, 2040